Monthly Notices
of the
ROYAL ASTRONOMICAL SOCIETY

MNRAS **452,** 998–1013 (2015) doi:10.1093/mnras/stv1271

Luminous red galaxies in clusters: central occupation, spatial distributions and miscentring

Hanako Hoshino,[1⋆] Alexie Leauthaud,[2⋆] Claire Lackner,[2] Chiaki Hikage,[3] Eduardo Rozo,[4] Eli Rykoff,[5] Rachel Mandelbaum,[6] Surhud More,[2] Anupreeta More,[2] Shun Saito[2] and Benedetta Vulcani[2]

[1]*Department of Physics and Astrophysics, Nagoya University, Aichi 464-8602, Japan*
[2]*Kavli IPMU (WPI), UTIAS, The University of Tokyo, Kashiwa, Chiba 277-8583, Japan*
[3]*Kobayashi-Maskawa Institute, Nagoya University, Nagoya 464-8602, Japan*
[4]*Department of Physics, University of Arizona, 1118 E. Fourth St., Tucson, AZ 85721, USA*
[5]*SLAC National Accelerator Laboratory, Menlo Park, CA 94025, USA*
[6]*McWilliams Center for Cosmology, Department of Physics, Carnegie Mellon University, 5000 Forbes Ave., Pittsburgh, PA 15213, USA*

Accepted 2015 June 4. Received 2015 June 4; in original form 2015 February 18

ABSTRACT

Luminous red galaxies (LRG) from the Sloan Digital Sky Survey are among the best understood samples of galaxies and are employed in a broad range of cosmological studies. In this paper, we study how LRGs occupy massive haloes via counts in clusters and reveal several unexpected trends. Using the red-sequence Matched-filter Probabilistic Percolation (redMaPPer) cluster catalogue, we derive the central occupation of LRGs as a function richness. We show that clusters contain a significantly lower fraction of central LRGs than predicted from the two-point correlation function. At halo masses of $10^{14.5}\,M_{\odot}$, we find $N_{\rm cen} = 0.73$ compared to $N_{\rm cen} = 0.89$ from correlation studies. Our central occupation function for LRGs converges to 0.95 at large halo masses. A strong anticorrelation between central luminosity and cluster mass at fixed richness is required to reconcile our results with those based on clustering studies. We derive the probability that the brightest cluster member is not the central galaxy. We find $P_{\rm BNC} \approx 20$–30 per cent which is a factor of $\sim$2 lower than the value found by Skibba et al. Finally, we study the radial offsets of bright non-central LRGs from cluster centres and show that bright non-central LRGs follow a different radial distribution compared to red cluster members. This work demonstrates that even the most massive clusters do not always have an LRG at the centre, and that the brightest galaxy in a cluster is not always the central galaxy.

Key words: galaxies: clusters: general.

1 INTRODUCTION

Luminous red galaxies (LRGs) are early-type massive galaxies consisting mainly of old stars with little ongoing star formation. Because LRGs are very luminous and can be detected to $z \sim 0.5$, they are commonly used for studies of large-scale structure. The Sloan Digital Sky Survey (SDSS; York et al. 2000) targeted a large sample of LRGs out to $z \sim 0.5$ using colour and magnitude cuts described in Eisenstein et al. (2001). LRGs from SDSS have been used for a wide variety of purposes, such as the detection of baryon acoustic oscillations (e.g. Eisenstein et al. 2005; Kazin et al. 2010), clustering studies (e.g. Zehavi et al. 2005; Padmanabhan et al. 2009; Reid & Spergel 2009; Parejko et al. 2013), weak lensing and cross-correlation studies (e.g. Mandelbaum et al. 2006; Hikage et al. 2013), and redshift space distortion (RSD) studies (Cabré & Gaztañaga 2009; Reid, Spergel & Bode 2009; Samushia, Percival & Raccanelli 2012; Hikage & Yamamoto 2013).

All of the studies described above require an understanding of how LRGs trace dark matter haloes, and, therefore, large-scale structure. One important aspect of how LRGs trace dark matter is how often they coincide with the centres of dark matter haloes. The identification of central galaxies in cluster samples is critical for a variety of studies, including the determination of cluster halo masses with weak gravitational lensing (George et al. 2012), and RSD studies (Hikage & Yamamoto 2013). Because LRGs are luminous and trace massive overdensities, it is often assumed that central galaxies are also LRGs. Indeed, in most galaxy clusters with at least one LRG, the brightest cluster galaxy (BCG) is an LRG. Furthermore, it is usually assumed that BCGs are *central* galaxies (van den Bosch et al. 2004; Weinmann et al. 2006; Budzynski et al.

⋆E-mail: hoshino.hanako@e.mbox.nagoya-u.ac.jp (HH); alexie.leauthaud@me.com (AL)

2012). However, recent results suggest that the central galaxy is not the BCG in all clusters (van den Bosch et al. 2005; Coziol et al. 2009; Sanderson, Edge & Smith 2009; Einasto et al. 2011, 2012; Skibba et al. 2011; Hikage et al. 2013; Sehgal et al. 2013; Lauer et al. 2014). For example, by analysing differences between the velocities and positions of BCGs relative to other cluster members, Skibba et al. (2011) found that 40 per cent of BCGs may in fact be satellite galaxies.

Knowing how LRGs occupy dark matter haloes, and especially whether or not the most dominant LRGs coincides with cluster centres, is of particular importance for RSD studies. Hikage & Yamamoto (2013) found that satellite LRGs have a significant effect on the higher order multipoles of the LRG power spectrum. This is simply due to the fact that satellite galaxies have large peculiar velocities that cause structures to be smeared out along the line-of-sight (the 'Finger-of-God' effect). Hence, understanding if LRGs trace halo centres and how often LRGs are satellites is an important ingredient for large-scale structure studies with LRG samples.

Halo occupation distribution (HOD) models (Peacock & Smith 2000; Seljak 2000; Scoccimarro et al. 2001; Berlind & Weinberg 2002) are the most popular framework for describing how LRGs populate dark matter haloes. The HOD model relies on the choice of a functional form for the probability that a halo of mass $M_{\rm h}$ contains N objects of a particular type ($P(N|M_{\rm h})$). This probability is typically divided into a contribution from central and from satellite galaxies. The mean probability for each component is the central occupation function, $N_{\rm cen}$, and the satellite occupation function, $N_{\rm sat}$, respectively. At group and cluster scales ($M_{\rm h} > 10^{14}\,{\rm M}_{\odot}$), the central occupation function of LRGs is often assumed to converge to unity. If this assumption is correct, then the central galaxies of massive haloes should all be LRGs. One of the primary goals of this paper is to test this assumption.

HOD models for LRGs are typically constrained by measurements of the LRG two-point correlation function (e.g. Zheng et al. 2005; Masjedi et al. 2006) or by using the counts-in-cylinders method developed by Reid & Spergel (2009). However, a complementary way to measure the HOD of LRGs is to directly count LRGs in clusters as a function of halo mass. For example, Ho et al. (2009) studied the HOD of LRGs using a sample of 47 clusters from the *Roentgen Satellite* (*ROSAT*) X-ray survey. The main caveat to this direct approach is that it relies on the availability of a trustworthy cluster catalogue with known centres and halo masses. Early cluster catalogues from SDSS such as MaxBCG (Koester et al. 2007) are known to have problems with centring. Johnston et al. (2007) estimate that the misidentification of centrals in the MaxBCG catalogue is roughly ∼30 per cent. Recently, however, much progress has been made in understanding how to improve centring algorithms for cluster finders (Rozo & Rykoff 2014; Rykoff et al. 2014).

The goal of this paper is to compare the central occupation function of LRGs as inferred from galaxy correlation measurements to direct counts of central LRGs in clusters. We use the red-sequence Matched-filter Probabilistic Percolation (redMaPPer) cluster catalogue (Rozo & Rykoff 2014; Rykoff et al. 2014), which includes carefully selected central galaxies based on luminosity, colour, and local galaxy density. One of the advantages of redMaPPer over previous cluster finders is that it adopts a probabilistic approach to cluster centring. This probabilistic approach is especially useful when, for example, two clusters are merging and when the central galaxy is not obvious. We caution that while the comparison of X-ray to optical centres in galaxy clusters so far suggests that the redMaPPer centring probabilities are accurate (Rozo & Rykoff 2014), the samples used in these comparisons are still small, and rely heavily on X-ray selected subsamples of clusters. More detailed investigation into the redMaPPer centring probabilities is still warranted, but for the purposes of this study we will assume the centring probabilities from the redMaPPer algorithm are correct. In Paper II, we perform additional tests on the redMaPPer centring probabilities by using weak gravitational lensing and cross-correlations. Preliminary results from this work indicate that the redMaPPer centroids are, on average, better indicators of halo centres than BCGs, adding confidence to the redMaPPer centring probabilities.

This paper is organized as follows. In Section 2 we briefly describe the redMaPPer cluster catalogue and our photometric SDSS LRG selection. In Section 3 we present the central occupation function of LRGs as inferred from the redMaPPer cluster catalogue, and compare four different definitions of the central galaxy. Our main results are presented in Section 3. Finally, we discuss the results and draw our conclusions in Sections 4 and 5, respectively.

Throughout this paper, we adopt a flat Λ cold dark matter (ΛCDM) cosmology with $h = 0.7$, $\Omega_{\rm m} = 0.25$, and $\sigma_8 = 0.8$. This cosmology is chosen for consistency with the redMaPPer richness–halo mass calibration in Rykoff et al. (2012). All distances are expressed in physical Mpc units. Halo mass is defined as $M_{200{\rm b}} \equiv M(< R_{200{\rm b}}) = 200\bar{\rho}\frac{4}{3}\pi R^3_{200{\rm b}}$, where $R_{200{\rm b}}$ is the radius at which the mean interior density is equal to 200 times the mean matter density ($\bar{\rho}$). All magnitudes are given on the AB system.

2 DATA

2.1 RedMaPPer cluster catalogue

The redMaPPer algorithm is a red-sequence-based cluster finder optimized for identifying clusters in large multiwavelength surveys. The details of the algorithm can be found in Rykoff et al. (2014) and Rozo & Rykoff (2014). Comparisons between redMaPPer and other cluster finding algorithms are performed in Rozo & Rykoff (2014) and Rozo et al. (2014a). The key elements of the redMaPPer algorithm are briefly summarized here. Using galaxies with spectroscopic redshifts, redMaPPer first constructs a red-sequence model as a function of luminosity and redshift. Once the red-sequence model is calibrated, redMaPPer then uses an iterative method to identify clusters assuming simple radial and luminosity filters. The redMaPPer algorithm is fully probabilistic. All potential cluster members are assigned a probability, $p_{\rm mem}$, of being a red cluster member. Cluster membership probabilities are tested using spectroscopic redshifts and are accurate to 1 per cent (Rozo et al. 2014b). Each cluster is assigned a photometric redshift, denoted z_λ, that is estimated from high-probability cluster members. Finally, redMaPPer estimates cluster richness (denoted λ) as the sum of membership probabilities over galaxies:

$$\lambda = \sum_i p_{{\rm free},i}\; p_{{\rm mem},i}\,, \tag{1}$$

where $p_{\rm free}$ represents the probability that a galaxy is not a member of another cluster (in general, $p_{\rm free} \approx 1$). The sum is performed over all galaxies within a characteristic cut-off radius, R_λ, which is a richness-dependent aperture that minimizes scatter in the mass–richness relation.

A key feature of the redMaPPer algorithm is that cluster centring is also probabilistic. For each cluster, redMaPPer provides a list of the five most likely central galaxies. Each of these five central galaxy candidates is assigned a probability, $P_{\rm cen}$, of being the cluster centre. Centring probabilities are defined using three filters: a luminosity

filter ($\phi_{\rm cen}$), a photometric redshift filter ($G_{\rm cen}$), and a local galaxy density filter ($f_{\rm cen}$). The product of these three terms determines the overall centring filter:

$$u_{\rm cen} = \phi_{\rm cen}(m_i|z_\lambda, \lambda) G_{\rm cen}(z_{\rm red}) f_{\rm cen}(w|z_\lambda, \lambda), \quad (2)$$

here m_i is the i-band apparent magnitude, $z_{\rm red}$ is the redshift of an individual galaxy (inferred from the colour), and w is the local galaxy density. An important point to note is that the redshift filter $G_{\rm cen}$ is broader than the cluster red-sequence filter and allows galaxies with slightly offset colours, and, therefore, lower $p_{\rm mem}$ values, to be considered central galaxy candidates. This allows for the possibility of residual amounts of star formation, and, therefore, bluer colours, in centrals. For each cluster, centring probabilities are normalized as

$$\sum_{i=1}^{5} P_{{\rm cen},i} = 1. \quad (3)$$

One consequence of equation (2) is that the brightest cluster member is not necessarily the galaxy with the highest value of $P_{\rm cen}$. This is because, in addition to luminosity, the central galaxy selection also considers local galaxy density via the $f_{\rm cen}$ filter. Hence, in some cases, a less luminous galaxy may have a higher centring probability because it is spatially coincident with the dense cluster core.

We use the redMaPPer v5.10 cluster catalogue (Rozo et al. 2014b) based on the SDSS Data Release 8 (DR8; Aihara et al. 2011). We select clusters in the range $\lambda > 20$ and $0.16 < z < 0.33$. The lower redshift limit, $z_{\rm min} = 0.16$, is set to avoid low redshifts where the LRG colour cuts begin to select a fainter population of galaxies (Eisenstein et al. 2001). The upper redshift limit, $z_{\rm max} = 0.33$, is set so that the resulting sample of clusters is volume limited. In addition, we select clusters for which less than 20 per cent of the cluster is masked (MASK_FRAC < 0.2). Altogether, there are 7730 clusters in this redshift and richness range.

Our SDSS DR8 redMaPPer cluster catalogue is limited to $i < 21.0$. This is roughly 1 mag deeper than LRG samples (see Section 2.3), ensuring that our cluster membership selection is complete for LRG-type galaxies.

2.2 Luminous red galaxies

LRGs are intrinsically red and bright galaxies selected from SDSS (Eisenstein et al. 2001). LRG samples extend fainter and farther than the SDSS main galaxy sample (Strauss et al. 2002) and consist of mainly passively evolving, massive, early-type galaxies with redshifts in the range $0.16 < z < 0.7$ (though we restrict the redshift range to $0.16 < z < 0.33$ here). In this paper, we will distinguish 'classical LRG' samples, which were targeted as part of the SDSS-I and SDSS-II programs (Eisenstein et al. 2001), from LRGs that were targeted as part of the SDSS-III Baryon Oscillation Spectroscopic Survey (BOSS) program (Dawson et al. 2013). We will refer to LRGs selected in SDSS-I and SDSS-II as 'classical LRGs'. We will use the term 'LOWZ' to refer to low-redshift ($z < 0.4$) LRGs from the SDSS-III BOSS program.

Fibre collisions occur because two fibres on the same SDSS spectroscopic plug plate (referred to as a 'tile') cannot be placed closer than 55 arcsec (SDSS-I/II) or 62 arcsec (SDSS-III). Large clusters may contain several LRGs and are hence more likely to be affected by fibre collisions than smaller systems, which have only one LRG. As a result, in the redMaPPer catalogue, 23 per cent of LRG cluster members lack a spectroscopic redshift. In order to circumvent this issue, we will use photometrically defined LRG samples. We use photometric data from SDSS DR8 for both the classical LRG and LOWZ selections.

In this paper, we consider the following three LRG samples.

(i) DR8PhotLRG: photometrically defined 'classical' LRGs selected from DR8 photometry.

(ii) DR8PhotLRG-MgCut: same as above but with an additional g-band absolute magnitude cut (see Section 2.3). We use this sample to compare with previous results derived from clustering studies.

(iii) PhotLOWZ: photometrically defined BOSS LOWZ sample selected from DR8 photometry.

We base our LRG selections on DR8 photometry but we note that subsets of the LRG samples were targeted based on photometry from earlier data releases. In Appendix A, we compare our samples based on DR8 photometry to LRG samples based on DR7 photometry and to the original spectroscopic target catalogues. In addition to covering a larger area than DR7, the DR8 photometry uses a new sky subtraction algorithm, affecting mainly bright galaxies ($r < 16$; Abazajian et al. 2009), and a new calibration (Padmanabhan et al. 2008). While the total numbers of LRGs selected using DR7 and DR8 photometry are the same, the actual galaxy samples differ at the $\sim$5 per cent level. This is due to scatter around the colour and magnitude cuts imposed by the LRG selections below. As we show in the Appendix A, the differences in photometry for LRGs are small (clipped rms $\delta m_r = 0.07$) and there are no systematic offsets in magnitudes or colour. The lack of systematic offsets suggests that the improved sky subtraction in DR8 has little effect on LRGs. This is expected since most LRGs are fainter than $r < 16$, where the effects of improved sky subtraction are most noticeable. Therefore, while the DR7- and DR8-selected LRG samples are not identical, they are comparable.

2.3 Classical LRGs and DR8PhotLRG cluster member selection

In this section we explain how we construct our sample of classical LRG cluster members, the 'DR8PhotLRG' sample. As stated in Section 2.1, we only consider cluster members with cluster redshifts in the range $0.16 < z < 0.33$. This redshift range is similar to the range considered for a variety of LRG studies: Zehavi et al. (2005) use $0.16 < z < 0.44$, Reid & Spergel (2009) use $0.16 < z < 0.36$, and Kazin et al. (2010) use $0.16 < z < 0.36$.

Classical LRGs are selected using a series of colour–colour and luminosity cuts in SDSS. Because the 4000 Å break moves from g- to r-band at $z \sim 0.4$, for classical LRGs there are two separate selections at redshifts above and below $z \sim 0.4$. The LRG selection at $z \lesssim 0.4$ is called 'Cut I'. Given our redshift range, in this paper, we only consider 'Cut I' LRGs. All colours are defined using model magnitudes[1] and all quantities are corrected for galactic extinction (Schlegel, Finkbeiner & Davis 1998).

We query the SDSS PHOTOPRIMARY table (see Appendix B for the full query) for all cluster members to obtain the photometric quantities necessary to apply the LRG 'Cut I' selection. Hereafter, the subscript 'mod' denotes model magnitudes, which are

[1] Note that model magnitude were improved in SDSS DR2 and later data releases. This caused changes in galaxy colours ($g_{\rm mod} - r_{\rm mod}$) and ($r_{\rm mod} - i_{\rm mod}$) of about 0.005 mag. The DR1 LRG selection criteria originally specified by Eisenstein et al. (2001) would lead to an increase in the LRG number density by about 10 per cent using DR2 photometry. To account for this, the LRG selection was slightly modified.

Table 1. Percentage of cluster members and central galaxies that fail to pass the LRG selection cuts given by equations (6)–(10). For example, among all 507 874 cluster member galaxies, 492 949 (97.1 per cent) do not satisfy equation (6), and 390 840 (77.0 per cent) do not satisfy equation (7). Each cut is applied separately in this table. Applying all of these cuts 12 001 cluster members (2.36 per cent) and 5823 central galaxies (75.3 per cent) are classified as LRGs.

LRG cut	Equation (6)	Equation (7)	Equation (8)	Equation (9)	Equation (10)
All cluster members	97.1	77.0	5.37	1.65	2.04
Most likely central galaxies	24.4	0.776	0.285	0.181	0.0129

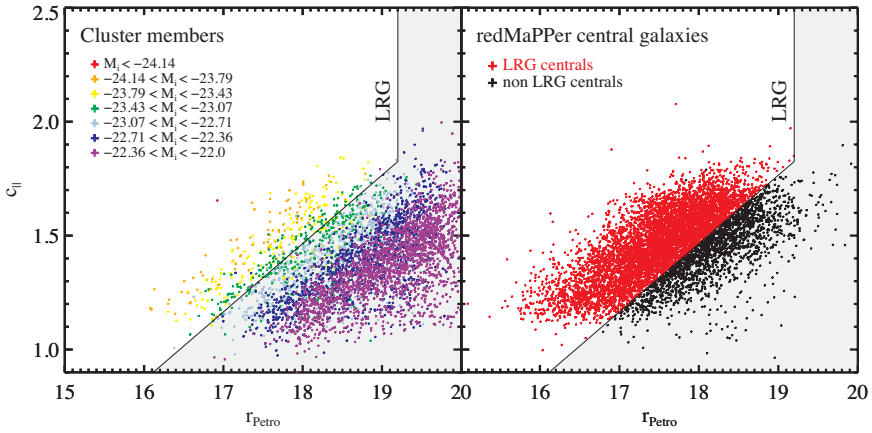

Figure 1. Left-hand panel: $c_\parallel$ as a function of Petrosian r-band magnitude, $r_{\rm Petro}$, for cluster members with $0.16 < z < 0.33$, $M_i < -22$, and $\lambda > 20$ (data points are randomly down-sampled for visual clarity). Cluster members are colour coded by their i-band absolute magnitude, M_i. The classical LRG cuts select cluster members brighter than $M_i \sim -23.2$. Among all cluster members, about 2 per cent are classified as LRGs. Right-hand panel: $c_\parallel$ versus $r_{\rm petro}$ for the *most likely* central galaxies chosen by redMaPPer. Red points show redMaPPer central galaxies that are LRGs while black points show centrals that fail the LRG selection. Most of the central galaxies in our sample that fail to pass the LRG cuts are intrinsically fainter than $M_i \sim -23.2$ (also see Fig. 4). Roughly 25 per cent of central galaxies in our cluster sample fail the LRG cuts. Central galaxies are primarily rejected from the LRG sample by equation (6).

derived by adopting the better fitting luminosity profile between a de Vaucouleurs and an exponential luminosity profile in the r band. The subscript 'cmod' denotes composite model magnitudes, which are calculated from the best-fitting linear combination of a de Vaucouleurs and an exponential luminosity profile. For classical LRGs, luminosity cuts are defined using $r_{\rm Petro}$, the Petrosian r-band magnitude. Two ancillary colours, $c_\perp$ and $c_\parallel$, are defined to align perpendicular and parallel to the locus of LRG galaxies in the ($g_{\rm mod} - r_{\rm mod}$, $r_{\rm mod} - i_{\rm mod}$) plane:

$$c_\perp = (r_{\rm mod} - i_{\rm mod}) - (g_{\rm mod} - r_{\rm mod})/4 - 0.177, \quad (4)$$

$$c_\parallel = 0.7(g_{\rm mod} - r_{\rm mod}) + 1.2[(r_{\rm mod} - i_{\rm mod}) - 0.177]. \quad (5)$$

Galaxies at $z \lesssim 0.4$ are distributed close to the linear locus $c_\perp = 0$, and $c_\parallel$ denotes where galaxies fall along this locus. Galaxies at higher redshifts have larger $c_\parallel$.

In this paper, we focus only on LRG samples at $z < 0.4$ which are selected via 'Cut I', as defined on the DR8 target selection webpage:[2]

$$r_{\rm Petro} < 13.116 + c_\parallel/0.3, \quad (6)$$

$$r_{\rm Petro} < 19.2, \quad (7)$$

$$|c_\perp| < 0.2, \quad (8)$$

$$\mu_{50} < 24.2\,{\rm mag\,arcsec^{-2}}, \quad (9)$$

$$r_{\rm psf} - r_{\rm mod} \geq 0.24, \quad (10)$$

where μ_{50} is the average surface brightness inside a Petrosian half-light radius, and $r_{\rm psf}$ is the point spread function (PSF) magnitude. Equation (6) ensures that the LRG sample has a roughly constant absolute magnitude limit in the range $0.16 < z < 0.4$. Equation (7) is set by the signal-to-noise ratio (S/N) requirement for spectroscopic redshift measurements using the SDSS telescope. The $c_\perp$ cut limits the redshift range to $z \lesssim 0.4$. The μ_{50} cut removes very low surface brightness objects, which may have odd colours. The final cut is a star–galaxy separator. As shown in Table 1, equations (6) and (7) have the most impact in defining the LRG cluster member sample. However, equation (7) only has a small impact on the LRG central sample simply because centrals are typically brighter than this limit.

With the extinction-corrected composite magnitudes, we calculate absolute magnitudes M_{ugriz} for cluster members as follows:

$$M_{ugriz} = m_{ugriz} - [k\text{-correction}] - [\text{distancemodulus}].$$

We use the software package K-CORRECT version 3.1 to perform this calculation (Blanton & Roweis 2007). To calculate the distance modulus, we use a spectroscopic redshift when it is available, otherwise we use the cluster redshift, z_λ. Absolute magnitudes derived with this equation are used in Figs 1, 2, and 4.

Fig. 1 illustrates how equations (6) and (7) operate. In this figure, we show how cluster members and central galaxies from our sample populate the $r_{\rm Petro}$ versus $c_\parallel$ plane. There are additional cuts that define LRGs (equations 8–10) but in practice these additional

[2] http://www.sdss3.org/dr8/algorithms/target_selection.php

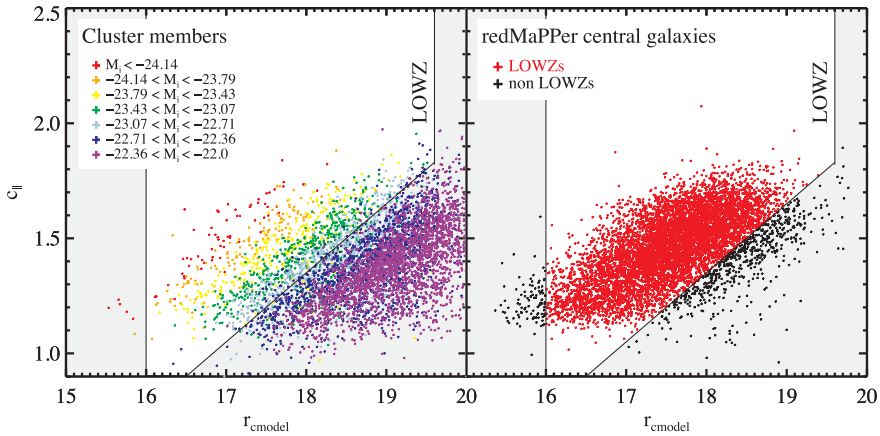

Figure 2. Same as Fig. 1 but for the BOSS LOWZ sample. Compared to classical LRGs, LOWZ galaxies extend to a fainter limit of $M_i \sim -22.8$. The right-hand panel shows that the LOWZ selection includes a bright cut at $r_{\rm cmod} > 16$, which excludes 1.3 per cent of the central galaxies in our sample.

cuts only play a minor role (see Table 1). The left-hand panel in Fig. 1 shows cluster members colour coded by absolute magnitude and illustrates that equation (6) (diagonal line) roughly selects a population of LRGs brighter than an absolute magnitude limit of $M_i \sim -23.2$. The right-hand side of Fig. 1 shows redMaPPer centrals (the most likely central galaxies according to redMaPPer). Roughly 25 per cent of redMaPPer centrals do not satisfy equations (6)–(10), mainly because they are fainter than $M_i \sim -23.2$.

In order to obtain a volume-limited LRG sample, clustering studies often apply an additional cut based on the g-band absolute magnitude, M_g (Zehavi et al. 2005; Reid & Spergel 2009; Kazin et al. 2010). After this M_g cut, the LRG number density[3] is $n_{\rm LRG} = 3.4 \times 10^{-5}$ Mpc^{-3}. To make our sample consistent with Reid & Spergel (2009), we apply a M_g cut of $-23.2 < M_g < -21.2$ to the 'DR8PhotLRG' sample to construct the 'DR8PhotLRG-Mgcut' sample. For consistency, we follow the same method to compute M_g[4] as in Kazin et al. (2010):[5]

$$M_g = r_{\rm Petro} - [\text{distancemodulus}] - \Delta g + (g - r) - z_{\rm calibration}. \quad (11)$$

Since the observed r-band is close to the rest-frame g band, $r_{\rm Petro}$ can be used to predict M_g. Δg and $(g - r)$ are colour and k-corrections from table 1 in Eisenstein et al. (2001), and $z_{\rm calibration} = 0.2$ accounts for evolution in the rest-frame colours from $z \sim 0.3$ to $z = 0$. We have checked that M_g derived in this fashion and derived from Kazin et al. (2010) yield similar results, despite the fact that Kazin et al. (2010) used DR7 photometry and we use DR8. We find the difference in M_g is small (rms $\delta M_g = 0.07$), consistent with the scatter in the photometry and that the differences in M_g do not affect the number of LRGs. Therefore, our results can be compared to results that directly use the Kazin et al. (2010) LRG selection.

[3] Our values assume $h = 0.7$. In h inverse units, the number density of classical LRGs is $n_{\rm LRG} = 1.0 \times 10^{-4}$ $(h^{-1}$ Mpc$)^{-3}$.
[4] When quoting values for M_i we assume $h = 0.7$. However, our M_g values assume h inverse units for consistency with Kazin et al. (2010) and Reid & Spergel (2009).
[5] http://cosmo.nyu.edu/~eak306/SDSS-LRG.html

2.4 BOSS LOWZ photometric cluster member selection

In this section we explain how we construct our sample of BOSS 'LOWZ' photometric cluster members (the 'PhotLOWZ' sample). The details of the LOWZ selection can be found in Dawson et al. (2013). The main difference between classical LRGs and LOWZs is that the BOSS selection extends about 0.4 mag deeper than the classical LRG selection. As a result, the LOWZ sample has a higher number density[6] than classical LRGs: $n_{\rm LOWZ} = 1.0 \times 10^{-4}$ Mpc^{-3}. In addition, the LOWZ selection includes a bright magnitude cut at $r_{\rm cmod} > 16$ which did not exist in the classical LRG selection. Finally, the LOWZ selection uses composite model magnitudes for magnitude cuts instead of Petrosian magnitudes.

Again, to avoid issues with fibre collisions, we define a photometric LOWZ sample. The ancillary colours $c_{\perp,\,\rm LOWZ}$ and $c_{\parallel,\,\rm LOWZ}$ are different than the classical LRG selection criteria:

$$c_{\perp,\rm LOWZ} = (r_{\rm mod} - i_{\rm mod}) - (g_{\rm mod} - r_{\rm mod})/4 - 0.18, \quad (12)$$

$$c_{\parallel,\rm LOWZ} = 0.7(g_{\rm mod} - r_{\rm mod}) + 1.2[(r_{\rm mod} - i_{\rm mod}) - 0.18]. \quad (13)$$

With these new definitions we select PhotLOWZ galaxies using these cuts:

$$r_{\rm cmod} < 13.5 + c_{\parallel}/0.3, \quad (14)$$

$$16 < r_{\rm cmod} < 19.6, \quad (15)$$

$$|c_{\perp}| < 0.2, \quad (16)$$

$$r_{\rm psf} - r_{\rm cmod} > 0.3. \quad (17)$$

As in the classical LRG selection, the $c_{\perp}$ cut crudely selects galaxies in the redshift range $z \lesssim 0.4$, equations (14) and (15) give an absolute magnitude and an apparent magnitude cut, respectively, and equation (17) is the star–galaxy separator. As shown in Table 2, equation (14) is the most stringent cut in defining the PhotLOWZ cluster member sample.

In Fig. 2 we illustrate how the LOWZ selection operates. As in Fig. 1, cluster members colour coded by absolute i-band magnitude are shown on the left and central galaxies are shown on the

[6] Our values assume $h = 0.7$. In h inverse units, the LOWZ number density is $n_{\rm LOWZ} = 3.0 \times 10^{-4}$ $(h^{-1}$ Mpc$)^{-3}$.

Table 2. Percentage of cluster members and central galaxies that fail to pass the LOWZ selection cuts given by equations (14)–(17). In total, before any cuts, there are 507 874 member galaxies and 7730 central galaxies. Among all the cluster members, 479 040 (94.3 per cent) do not satisfy equation (14) and 316 028 (62.2 per cent) do not satisfy equation (15). Applying all of these cuts, 24 761 cluster members (4.88 per cent) and 7001 central galaxies (90.6 per cent) are classified as LOWZs.

LOWZ cut	Equation (14)	Equation (15)	Equation (16)	Equation (17)
All cluster members	94.3	62.2	5.37	4.74
Most likely central galaxies	7.84	1.54	0.285	0.0259

right. Absolute magnitudes are calculated in the same way as in Section 2.3. As can be seen by comparing Figs 1 and 2, the LOWZ selection reaches ∼0.3 mag fainter in the i band than the classical LRG selection. At the bright end, 1.3 per cent (100 galaxies) of the most likely redMaPPer central galaxies are rejected by the $r_{\rm cmod} > 16$ cut.

2.5 Selecting LRGs in clusters

For most of our calculations, we consider all LRGs in a cluster with non-zero membership probability, which we will call the '*probabilistic-sample*'. When using this sample, our calculations will account for membership probabilities by summing over $p_{\rm mem}$ values.

However, in some cases it is useful to have a deterministic sample of LRGs in clusters (e.g. for plotting). In such cases, we select the λ most likely cluster members for each cluster (λ is rounded to the nearest integer). We will call this the '*fixed-sample*'. We will clarify in the text when each of these samples is considered. When using the fixed sample, the galaxy with the highest value of $P_{\rm cen}$ is called the redMaPPer central.

3 RESULTS

In this section we investigate two questions: (i) How often are central galaxies LRGs? and (ii) How often are central galaxies also the brightest LRGs in each cluster? For most of our calculations, we treat cluster centres and member galaxies probabilistically and use the centring probability, $P_{\rm cen}$, and the membership probability, $p_{\rm mem}$.

3.1 Cluster centroids

We consider four different cluster centroids.

(i) *RMCG*. The redMaPPer central galaxy. For each cluster, this is the galaxy with the highest value of $P_{\rm cen}$. This is the galaxy that redMaPPer selects as the most likely centre for each cluster.

(ii) *BMEM*. The brightest red-sequence cluster member identified by redMaPPer, where brightness is given by $i_{\rm cmod}$. In most cases, this is defined with the *probabilistic-sample* and treated probabilistically according to the $p_{\rm mem}$ values. In some cases, BMEM will be defined using the *fixed-sample* (we clarify in each case which definition is used).

(iii) *BLRG*. The brightest DR8PhotLRG in each cluster (if the cluster has at least one DR8PhotLRG). This is defined in a similar fashion as BMEM.

(iv) *BLOWZ*. The brightest PhotLOWZ in each cluster (if the cluster has at least one PhotLOWZ). This is defined in a similar fashion as BMEM.

Table 3. Per cent of time when two of samples (i)–(iv) overlap. For example, in clusters that have at least one LRG, 84.1 per cent of BLRGs are also RMCGs. In clusters that have at least one LRG/LOWZ, 94.7 per cent of BLOWZ are also BLRGs. Here, BLRG, BLOWZ, and BMEM are defined using the '*fixed-sample*'.

	RMCG	BLRG	BLOWZ	BMEM
RMCG	100	84.1	80.1	80.5
BLRG	–	100	94.7	95.5
BLOWZ	–	–	100	96.3
BMEM	–	–	–	100

Note that RMCG is defined as the galaxy with the highest value of $P_{\rm cen}$, but that the actual centring probability of RMCG galaxies may be less than 1. In our sample, RMCGs have $P_{\rm cen}$ values between 0.27 and ∼1.00 with a mean value of $\langle P_{\rm cen}\rangle = 0.87$. Hence, RMCGs may not always be the true cluster centre. Indeed, redMaPPer predicts that 13 per cent of RMCGs will not be a true cluster centre.

We show a simple comparison between these different classifications in Table 3. We use the '*fixed-sample*' (see Section 2.5 for the sample definition) to define BLRGs, BLOWZs, and BMEMs.

3.2 Central occupation functions of LRGs and LOWZ galaxies

We now compute the probability that a cluster of richness λ hosts a central galaxy that is also an LRG or a LOWZ galaxy. When expressed as a function of halo mass, this is known as the LRG/LOWZ central occupation function, $N_{\rm cen}(M_{\rm 200b})$. To begin with, we compute $N_{\rm cen}$ as a function of cluster richness. To measure $N_{\rm cen}(\lambda)$, we use the '*probabilistic-sample*' where the sum of $P_{\rm cen}$ for each cluster is equal to 1.

We use 10 bins in cluster richness from $\lambda = 20$ to 150. In each richness bin, we measure the mean value of $P_{\rm cen}$ for all LRG (or LOWZ) members. For any given cluster, the total value of $P_{\rm cen}$ summed over LRG members represents the probability that the central galaxy of that cluster is an LRG. In the jth bin, $N_{\rm cen}(\lambda)$ is

$$\langle N_{\rm cen}(\lambda)\rangle_j = \frac{1}{n_{{\rm clus},j}(\lambda)} \sum_i P^{\rm LRG}_{{\rm cen},i}, \quad (18)$$

where $n_{{\rm clus},j}(\lambda)$ is the number of clusters in the jth richness bin, and the subscript i denotes all LRG cluster members in this richness bin.

The results for $N_{\rm cen}(\lambda)$ are shown in the two left-hand panels of Fig. 3. Errors are calculated via bootstrap. For consistency with Reid & Spergel (2009), we apply a g-band absolute magnitude cut to our LRG sample (we use the 'DR8PhotLRG-Mgcut' sample, see Section 2.3). For both LRGs and LOWZ galaxies, we find that $N_{\rm cen}(\lambda)$ does not converge to 1 for large values of λ. Instead, $N_{\rm cen}(\lambda)$ flattens and converges to ∼0.9 at $\lambda = 150$.

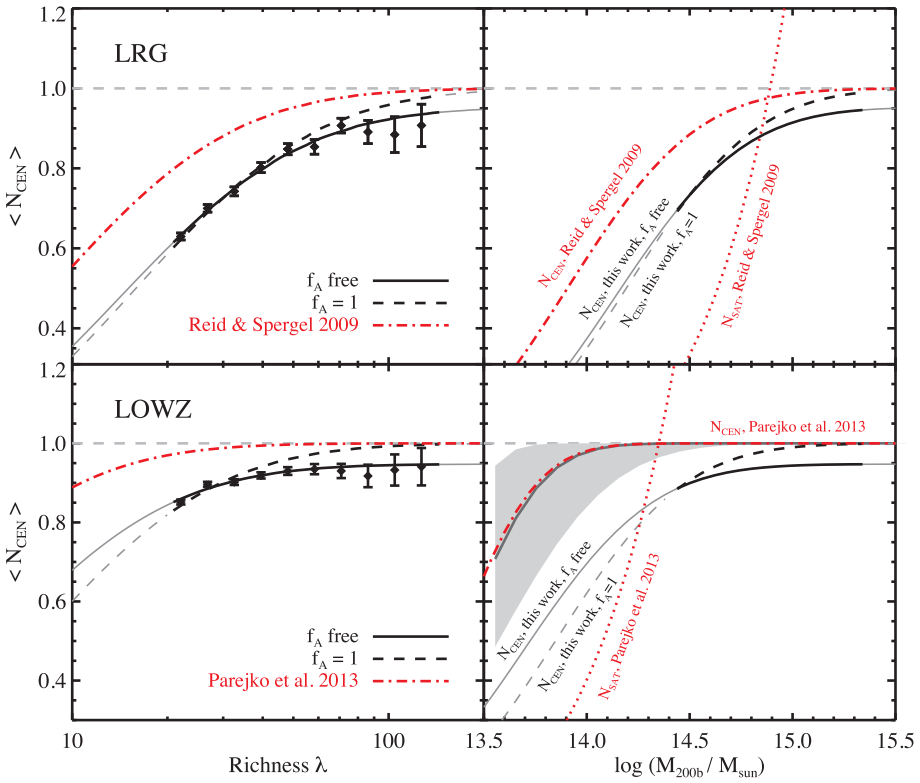

Figure 3. Left-hand panels: $N_{\rm cen}(\lambda)$ for LRGs (upper panel) and for LOWZ galaxies (lower panel). Solid black lines show our best fit to $N_{\rm cen}(\lambda)$ when f_A is left as a free parameter, and the black dashed lines show the best fit when $f_A = 1$. Red dash–dotted lines are the results from Reid & Spergel (2009) and Parejko et al. (2013) that have been converted to $N_{\rm cen}(\lambda)$ using equation (23). Right-hand panels: $N_{\rm cen}(M_{200b})$ inferred by fitting equation (23) to the measured $N_{\rm cen}(\lambda)$. Solid black lines show our results when f_A is a free parameter. The thick black portion of the curve corresponds to the region constrained by the cluster data. Black dashed lines show our results when $f_A = 1$. Red dash–dotted lines correspond to $\langle N_{\rm cen}\rangle$ and red dotted lines correspond to $\langle N_{\rm sat}\rangle$ from Reid & Spergel (2009) (top) and Parejko et al. (2013) (bottom). The grey solid line in the lower right-hand panel shows $N_{\rm cen}(M_{200b})$ we obtain by refitting the data points from Parejko et al. (2013). The 68 per cent confidence region for this fit is shown using grey shaded regions. For both LRGs and LOWZs, we find a significant difference between the normalization of $N_{\rm cen}$ inferred from direct counts in clusters and that from HOD modelling of the two-point correlation function (compare black lines to red dash–dot lines).

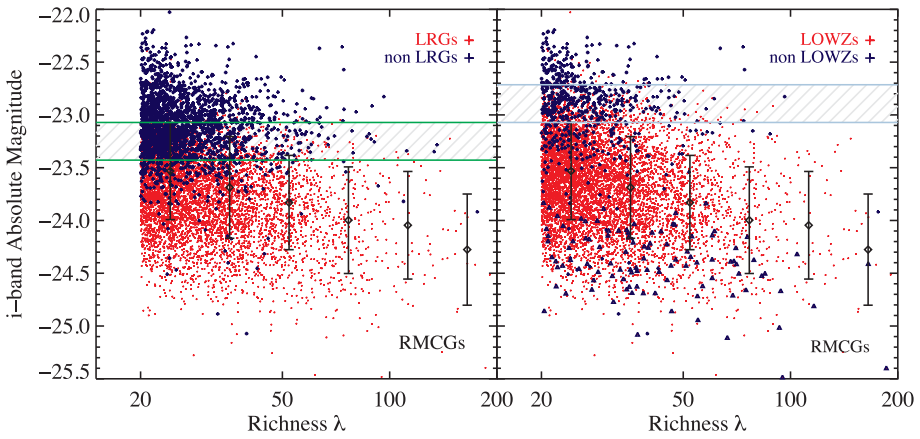

Figure 4. Left-hand panel: *i*-band absolute magnitude of central galaxies as a function of cluster richness. Red points represent RMCGs that are also DR8PhotLRGs. Small dark blue points show RMCGs that fail to pass our photometric LRG selection. Open black diamonds with error bars show the mean magnitude in each richness bin with errors that represent the standard deviation of the distribution in each bin. The green shaded region is the approximate *i*-band magnitude limit that defines the LRG selection ($-23.43 \lesssim M_i \lesssim 23.07$, see Fig. 1). At $\lambda < 40$, many RMCGs are simply too faint to pass the LRG cut, and there are excluded faint RMCGs at larger richness as well. Right-hand panel: similar plot as in the left-hand panel using the LOWZ selection criteria. Red points represent RMCGs that are also PhotLOWZs, and black points represent RMCGs that are not PhotLOWZs. Filled blue triangles are RMCGs that are not PhotLOWZs because they are brighter than $r_{\rm cmod} = 16$. The light-blue horizontal band shows the absolute *i*-band magnitude cut that roughly defines the LOWZ selection ($-23.07 \lesssim M_i \lesssim -22.71$).

Table 4. HOD fits to $N_{\rm cen}(\lambda)$ for the DR8PhotLRG-Mgcut sample and the PhotLOWZ sample. We fit $N_{\rm cen}(\lambda)$ both fixing $f_A = 1$ and allowing f_A to be a free parameter. The last two columns in this table are derived and discussed in Section 4.

	f_A	$\log(M_{\rm min}/{\rm M}_\odot)$	χ^2/dof	$n_{\rm CEN}$ (Mpc^{-3})	Implied satellite fraction
LRG	1.0 (fixed)	14.19 ± 0.01	$15.1/9 = 1.7$	1.8×10^{-5}	47 per cent
LRG	0.953 ± 0.014	14.14 ± 0.02	$4.87/8 = 0.61$	1.9×10^{-5}	44 per cent
LOWZ	1.0 (fixed)	13.85 ± 0.01	$53.8/9 = 5.9$	3.5×10^{-5}	65 per cent
LOWZ	0.947 ± 0.007	13.69 ± 0.03	$15.2/8 = 1.9$	4.2×10^{-5}	58 per cent

3.2.1 *Non-LRG redMaPPer centrals*

The fact that $N_{\rm cen}(\lambda)$ does not converge to 1 even for large values of λ can be explained by Fig. 4. This figure shows the *i*-band absolute magnitude distribution of the most likely RMCGs as a function of cluster richness. As expected, the absolute magnitudes are correlated with richness: brighter galaxies tend to be in richer clusters. However, there is significant scatter in this relation. The rms dispersion of M_i as a function of λ is $\sigma_{M_i} \sim 0.50$ for all RMCGs and $\sigma_{M_i} \sim 0.46$ for RMCGs with $P_{\rm cen} > 0.99$. The dispersion does not depend strongly on λ. These values are similar to those reported by Hansen et al. (2005) for the MaxBCG cluster finder ($\sigma_{\log_{10}(L_i)} = 0.17$, or $\sigma_{M_i} = 0.425$). In Section 2.2, we show that the LRG cuts roughly select galaxies above a fixed absolute magnitude threshold. This is shown by green horizontal lines in Fig. 4. Because of the trend with M_i and the significant scatter in M_i, a sizable fraction (28 per cent) of RMCGs in clusters with $\lambda < 40$ are simply too faint to pass the LRG cuts. The scatter in M_i at fixed halo mass also means there is a non-negligible fraction of faint central galaxies in rich, massive haloes that fail to pass the LRG cuts.

The right-hand side of Fig. 4 paints a similar picture for LOWZ galaxies. The main difference is that the LOWZ selection extends to fainter absolute magnitudes so a larger number of RMCGs are also PhotLOWZs. There is however, one additional difference due to the bright *r*-band cut applied for the LOWZ selection (see equation 15 in Section 2.4). This cut excludes about 102 bright central galaxies (these have a mean *r*-band magnitude of $\langle r_{\rm cmod}\rangle = 15.8$). For some studies, it may be desirable to add these bright galaxies back in so as to remove the effects of the LOWZ bright cut. Indeed, many of these very bright galaxies are already targeted as main sample galaxies or as classical LRGs.[7] Among the 102 bright RMCGs in our sample that do not pass the LOWZ cut, 73 have spectroscopic redshifts in DR10. These missing galaxies contribute to the low $N_{\rm cen}(\lambda)$ at high halo mass shown in Fig. 3.

3.2.2 *Converting* $\rm N_{cen}(\lambda)$ *to* $\rm N_{cen}(M_{200b})$

We now convert $N_{\rm cen}(\lambda)$ to $N_{\rm cen}(M_{\rm 200b})$ to compare with results derived from HOD modelling of counts-in-cylinders and the two-point correlation function (Reid & Spergel 2009; Parejko et al. 2013). In order to convert λ to halo mass, we adopt the richness–halo mass relation from Rykoff et al. (2012). In Section 4, we perform tests to evaluate the impact of the uncertainty in this relation on our results. In Rykoff et al. (2012), the probability that a cluster of richness λ has mass $M_{\rm 200b}$, $P(M_{\rm 200b}|\lambda)$, is assumed to follow a log-normal distribution with a scatter of $\sigma_{M|\lambda} = 0.25$. The mean of this log-normal relation is given by

$$\ln\left(\frac{M_{\rm 200b}}{h_{70}^{-1}10^{14}\,{\rm M}_\odot}\right) = 1.72 + 1.08\ln\left(\frac{\lambda}{60}\right). \quad (19)$$

Using this conversion, our lower richness limit of $\lambda = 20$ corresponds to a halo mass of $M_{\rm 200b} = 2.44 \times 10^{14}\,{\rm M}_\odot$ and a richness of $\lambda = 100$ corresponds to a halo mass of $M_{\rm 200b} = 1.39 \times 10^{15}\,{\rm M}_\odot$.

Rykoff et al. (2012) specify $P(M_{\rm 200b}|\lambda)$ but $P(\lambda|M_{\rm 200b})$ is more useful for our calculations. We derive $P(\lambda|M_{\rm 200b})$ following the method described in the appendix of Leauthaud et al. (2010) which assumes that $P(\lambda|M_{\rm 200b})$ is also a log-normal of the form

$$P(\lambda|M_{\rm 200b}) = \frac{1}{\sqrt{2\pi}\sigma_{\lambda|M}}\exp\left[-\frac{(\ln\lambda - \ln\lambda_{\rm mean}(M_{\rm 200b}))^2}{2\sigma^2_{\lambda|M}}\right]. \quad (20)$$

For this calculation we adopt the halo mass function from Tinker et al. (2008). From equation (20) and the halo mass function, we find $\sigma_{\lambda|M} = 0.231$ and

$$\ln\lambda_{\rm mean}(M_{\rm 200b}) = 0.925\ln\left(\frac{M_{\rm 200b}}{{\rm M}_\odot}\right) - 28.26. \quad (21)$$

With this relation in hand, we now convert $N_{\rm cen}(\lambda)$ to $N_{\rm cen}(M_{\rm 200b})$. For this purpose, we assume that $N_{\rm cen}(M_{\rm 200b})$ follows the functional form

$$\langle N_{\rm cen}(M_{\rm 200b})\rangle = \frac{f_A}{2}\left[1 + {\rm erf}\left(\frac{\log_{10}(M_{\rm 200b}/M_{\rm min})}{\sigma_{\log M}}\right)\right]. \quad (22)$$

This functional form for $N_{\rm cen}$ is similar to that in Reid & Spergel (2009) but with an extra free parameter, f_A, which allows $N_{\rm cen}$ to converge to values less than unity at large halo masses.

Given equation (20) and assuming the Tinker et al. (2008) halo mass function $\frac{{\rm d}n}{{\rm d}m}$ at $z = 0.2$, $N_{\rm cen}(\lambda)$ is computed as

$$N_{\rm cen}(\lambda) = \frac{\int P(\lambda|M_{\rm 200b})N_{\rm cen}(M_{\rm 200b})\frac{{\rm d}n}{{\rm d}m}(M_{\rm 200b}){\rm d}M_{\rm 200b}}{\int P(\lambda|M_{\rm 200b})\frac{{\rm d}n}{{\rm d}m}(M_{\rm 200b}){\rm d}M_{\rm 200b}}. \quad (23)$$

We fit our measurements of $N_{\rm cen}(\lambda)$ using equation (23) with free parameters f_A and $M_{\rm min}$. The best-fitting parameters are given in Table 4. The parameter $\sigma_{\log M}$ is fixed to 0.7, which corresponds to the value found by Reid & Spergel (2009). The cluster sample used in this paper ($\lambda > 20$) does not extend to low enough halo masses to fully constrain $\sigma_{\log M}$. However, the redMaPPercluster catalogue does extend to $\lambda > 5$, which could help constrain $\sigma_{\log M}$ in future work.

3.2.3 *Comparison with Reid & Spergel (2009) and Parejko et al. (2013)*

In Fig. 3, we compare our $N_{\rm cen}(M_{\rm 200b})$ with the central occupation function derived by Reid & Spergel (2009), who used a combination of clustering and the counts-in-cylinders technique to constrain the

[7] This will not be true for parts of the Southern Galactic Cap that were extended by the BOSS survey.

HOD of LRGs. The halo mass definition assumed in Reid & Spergel (2009) is the same as this work.[8] The Reid & Spergel (2009) results use haloes identified by a spherical overdensity algorithm and so will be comparable with the redMaPPer cluster finder.

For LOWZ, we compare with $N_{\rm cen}$ derived by Parejko et al. (2013). Because Parejko et al. (2013) use friend-of-friend (FOF) haloes, their results are not directly comparable to ours. We take two measures to account for this difference. First, we convert the Parejko et al. (2013) results to our halo mass definition[9] following More et al. (2011). Second, we refit the measurements of abundance and clustering of LOWZ galaxies presented by Parejko et al. (2013). For this, we use the analytical framework for the halo occupation distribution developed in van den Bosch et al. (2013), which accounts for the radial dependence of the bias, halo exclusion, and redshift space distortion effects on the projected clustering of galaxies (see also Cacciato et al. 2013; More et al. 2013). In fitting the clustering data, we use the parametrization as Parejko et al. (2013) (see also Miyatake et al. 2013; More et al. 2014). We adopt a consistent halo mass definition of $M_{\rm 200b}$ while performing the fits so that the HOD modelling results can be directly compared with the results from our cluster catalogue. The 68 and 95 per cent confidence regions are shown using grey shaded regions in Fig. 3. Our refits to the Parejko et al. (2013) data points are in excellent agreement with Parejko et al. (2013) HOD after converting to a single halo mass definition, suggesting that differences between FOF haloes and spherical overdensity haloes do not have a large impact on $N_{\rm cen}$.

For both the LRG sample and the LOWZ sample, we find significant differences in the amplitude of $N_{\rm cen}$ derived from HOD modelling of LRG/LOWZ clustering and derived directly from the redMaPPer cluster catalogue. Possible explanations for this discrepancy are presented in Section 4.

3.3 How often is the brightest LRG not the central galaxy?

Although many studies assume that the brightest galaxy in a cluster is also the central galaxy (van den Bosch et al. 2004; Weinmann et al. 2006; Budzynski et al. 2012), some recent studies suggest that is not always the case (van den Bosch et al. 2005; Coziol et al. 2009; Sanderson et al. 2009; Hikage et al. 2013). Because redMaPPer uses colour and position in addition to luminosity to determine which galaxy is the central galaxy, we can test this assumption by calculating the probability that the brightest LRG/LOWZ galaxy in a cluster is not the central galaxy (denoted $P_{\rm BNC}$). To compute $P_{\rm BNC}$, we follow the probabilistic method outlined in Reddick et al. (in preparation). For each cluster, we identify all LRGs brighter than the ith candidate central. $P_{\rm BNC}$ for LRG is computed as

$$P_{\rm BNC} = \sum_{i=1}^{5} P_{{\rm cen},i} \sum_{j} P_{{\rm mem},j} \prod_{k} (1 - P_{{\rm mem},k}). \quad (24)$$

The first sum runs over all five candidate centrals, not limited to LRGs. The second sum over j is for all LRGs that are brighter than central candidate i. The final product over k is for LRG members brighter than galaxy j to ensure that only the BLRG is considered.

[8] The HOD parameters given in Reid & Spergel (2009) assume $h = 0.7$. We have checked that integrating the Reid & Spergel (2009) HOD with $h = 0.7$ yields the correct LRG number density.

[9] The FOF halo masses roughly correspond to an overdensity of 500 times the mean matter density (More et al. 2011). We convert the FOF halo masses from Parejko et al. (2013) to our halo mass convention assuming that $M_{\rm 200b}/M_{\rm 500b} = 1.32$.

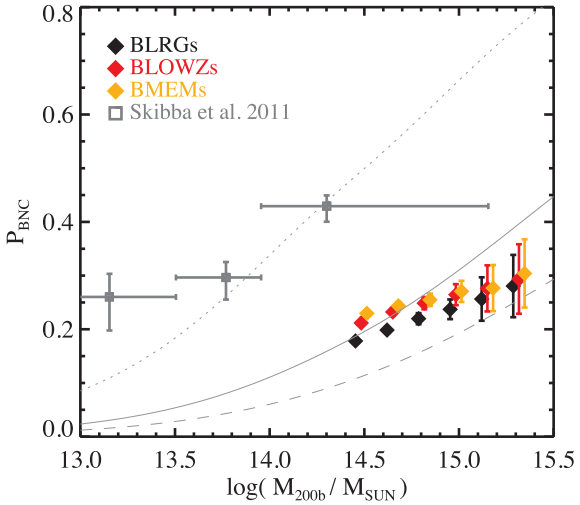

Figure 5. Probability that there exists a redMaPPer cluster member (orange), an LRG member (black), or a LOWZ member (red), that is brighter than the central galaxy as a function of halo mass. Errors are derived via bootstrap. Grey points show measurements from Skibba et al. (2011). Grey lines show predictions from Skibba et al. (2011) based on the conditional luminosity function (CLF) from Cacciato et al. 2009, and assuming three different values for the slope in the satellite CLF ($s = 1$ dotted curve, $s = 2$ solid curve, $s = 3$ dashed curve)

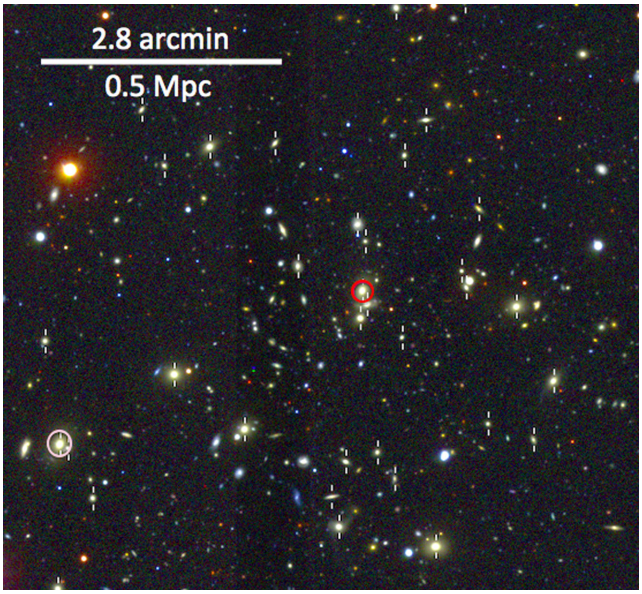

Figure 6. SDSS image of a cluster in which the redMaPPer central galaxy is not the brightest member. Member galaxies are shown with white ticks. The richness of this cluster is $\lambda = 54.8$. The galaxy circled in red in the middle is the most likely central, and the one circled in pink (lower left) is the brightest member. The centring probability of the central galaxy is 0.930. The brightest member of this cluster has $P_{\rm cen} = 0.0$. The i-band apparent magnitudes of the central galaxy and the brightest member are $m_i = 16.8$ and $m_i = 16.3$, respectively.

Fig. 5 shows the mean probability that the BLRG or BLOWZ galaxy in a cluster is not the central galaxy. We find that $P_{\rm BNC}$ varies between 0.2 and 0.3 and mildly increases with halo mass. Fig. 6 shows an example of a cluster in which the central galaxy is not the brightest member. The most likely central galaxy of this

cluster has $P_{\rm cen} = 0.930$, and the $P_{\rm cen}$ value for the brightest galaxy (in the *fixed-sample*) is 0. The central is not an LRG but the brightest member is an LRG. In this cluster, the BLRG is less likely to be the central because it is offset from most other cluster members.

We compare our results with Skibba et al. (2011) in Fig. 5. Skibba et al. (2011) compute $P_{\rm BNC}$ by comparing the velocity and positional offsets of the brightest cluster galaxy from the other cluster members to the expected offsets computed using mock group catalogues. The Skibba et al. (2011) results are derived from the Yang et al. (2007) group catalogue. The details of the cluster finding algorithm are accounted for in the Skibba et al. (2011) analysis by running the Yang et al. (2007) group finder on mock catalogues. Note that the Skibba et al. (2011) results span a lower redshift range ($0.01 < z < 0.20$), and larger halo mass range ($12 < \log(M_{\rm halo}/{\rm M}_\odot) < 15$) than our results. We convert the Skibba et al. (2011) results to our assumed value of $h = 0.7$. We do not, however, account for the difference in halo mass definition, M_{180b} in Skibba et al. (2011) versus M_{200b} here, as the correction is of order 3 per cent.

Our values of $P_{\rm BNC}$ are significantly lower than those found by Skibba et al. (2011). At a halo mass of $\log(M_{180b}/{\rm M}_\odot) = 14.29$, Skibba et al. (2011) find $P_{\rm BNC} = 0.43$, whereas we find $P_{\rm BNC} = 0.23$ at $\log(M_{200b}/{\rm M}_\odot) = 14.5$. As demonstrated in Reddick et al. (in preparation), part of the difference may be explained by a tendency to oversubtract the sky around bright, extended galaxies in SDSS data releases prior to DR8. While we rely on DR8 data, Skibba et al. (2011) use SDSS DR4 photometry. Improvements in the sky subtraction in DR8 typically increased the measured luminosities of central galaxies more than those of satellites (Bernardi et al. 2013), thus decreasing the probability that a satellite is brighter than the central galaxy. However, the sky subtraction is most relevant at redshifts below the range we study here, and may only explain part of the discrepancy. We refer to Reddick et al. (in preparation) for further details on this question.

In conclusion, we find that within the redMaPPer cluster catalogue, the brightest LRG/LOWZ galaxy is also the central galaxy in only ∼70 per cent of clusters. This will impact redshift space distortions (RSD) studies that construct 'halo catalogues' under the assumption that the brightest LRG is always the central galaxy (Hikage & Yamamoto 2013). This also suggests that naive cluster-finding algorithms that assume the central galaxy is the brightest galaxy in a cluster may have a 20–30 per cent miscentring fraction (van den Bosch et al. 2005; Coziol et al. 2009; Sanderson et al. 2009).

3.4 Offset distributions between the central galaxy and the brightest LRG

We now investigate how the radial distributions of non-central BLRGs compare with the radial distributions of red cluster members. We compute the distribution of projected offsets between the brightest and central galaxies for clusters in which the BLRG is not the central galaxy. Specifically, we compute $D_{\rm off}/R_\lambda$, where $D_{\rm off}$ represents the 2D projected distance between the central galaxy and the BLRG/BLOWZ. We normalize $D_{\rm off}$ by the cluster cut-off radius, R_λ, to account for size variations among clusters. $D_{\rm off}$ is computed as follows. For each cluster, we consider all five central galaxy candidates. Let us consider the ith central candidate with a centring probability of $P_{{\rm cen},\,i}$. We identify all LRG cluster members brighter than central galaxy i. The probability of observing an offset

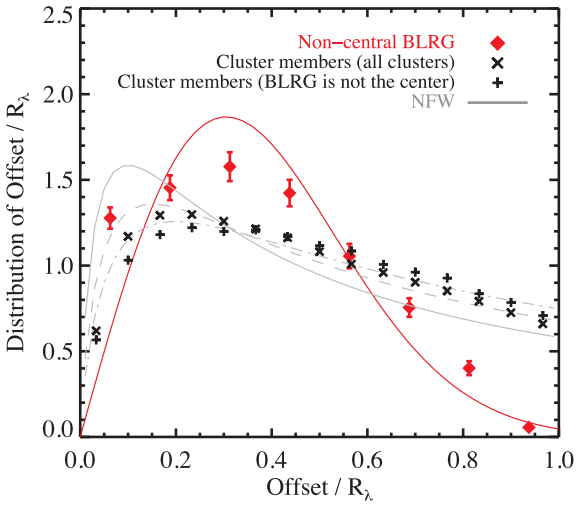

Figure 7. Distribution of $D_{\rm off}/R_\lambda$ for the brightest LRGs, when the RMCG and BLRG are different. Errors are calculated by bootstrap. The red solid curve shows the best fit assuming a Rayleigh distribution. Black crosses represent the distribution of all redMaPPer cluster members. Black plus signs represent the distribution of all redMaPPer cluster members in clusters in which the BLRGs are not the central galaxies. The fact that the black crosses and black plus signs trace similar distributions suggests that clusters with non-central BLRGs are not dominated by projection effects and/or mergers. Grey curves represent the expected distribution of satellites distributed according to NFW profiles with different halo masses at redshift $z = 0.25$. Grey solid, dashed, and dash–dotted curves are $\log(M_{200b}) = 14.0$, 14.5, and 15.0, respectively (and the halo concentrations are $c = 7.2$, 6.5, and 5.3). The distribution of $D_{\rm off}/R_\lambda$ for non-central BLRGs is significantly different (truncated at the outskirts) compared to the distribution for all cluster members.

$D_{{\rm off},\,ij}$ between central galaxy i and the brightest LRG j in the cluster is

$$P(D_{{\rm off},ij}) = P_{{\rm cen},i}\,P_{{\rm mem},j}\prod_k(1 - P_{{\rm mem},k}), \qquad (25)$$

which is simply the i, jth term in the sum making $P_{\rm BNC}$ (see equation 24).

Fig. 7 is constructed by finding all configurations in which LRG j is brighter than central galaxy i and computing $D_{{\rm off},\,ij}$ and $P(D_{{\rm off},\,ij})$. We then bin the $D_{\rm off}/R_\lambda$ values and sum the $P(D_{{\rm off},\,ij})$ values in each bin. We only show the distribution of offsets for BLRGs, because the distributions are similar for BLOWZ galaxies and BMEM galaxies. The mean offset between the RMCG and the brightest LRG (when these galaxies differ) is $0.4R_\lambda$.

For reference, we show the expected distribution of $D_{\rm off}/R_\lambda$ assuming a Navarro–Frenk–White (NFW) profile (grey lines). This is computed by first integrating the three-dimensional density profile along the line-of-sight to obtain the projected surface mass density. The curves are then computed by multiplying the area of a thin annulus at each radius to the density at each radius. Each grey line shows a different halo mass and halo concentration. Fig. 7 shows that the distribution of 2D projected halocentric distances to BLRGs is significantly different (more truncated at the outskirts) than the distribution of radial distances to all cluster members. The differences between these distributions may indicate a larger impact of dynamical friction on more massive subhaloes as suggested by Wu et al. (2013). Fig. 7 also shows that the distribution of radial offsets for member galaxies in clusters is the same whether or not the

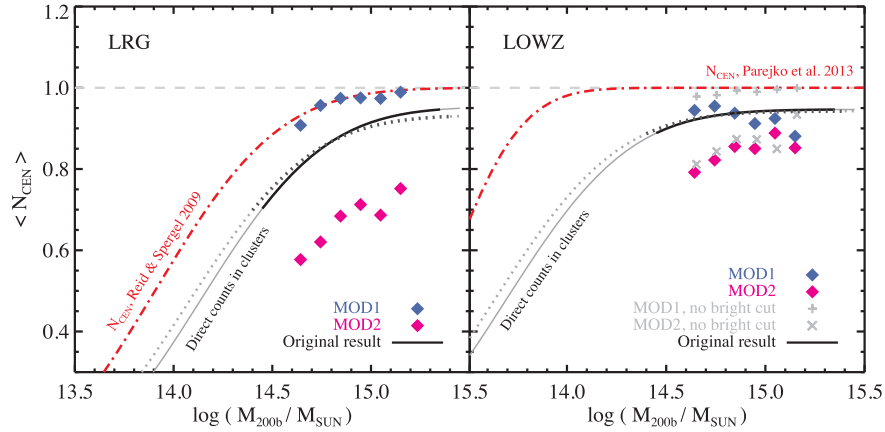

Figure 8. Tests to explain the origin of the $N_{\rm cen}(M_{\rm 200b})$ discrepancy. Our original results from Fig. 3 are shown with black/grey solid curves. First, we test the impact of the mass–richness relation. The dotted grey lines show $N_{\rm cen}(M_{\rm 200b})$ inferred using an updated mass–richness relation with a slope of 1.2, instead of 1.08, in equation (19). The updated mass–richness relation only has a minor impact on our results. Second, we test if correlations between halo mass, richness, and magnitude of the central galaxy may impact our results. In both panels, the blue data points show MOD1, in which halo mass and central galaxy luminosity are correlated at fixed richness (or brighter centrals live in less rich clusters at fixed halo mass). The magenta points show MOD2, in which halo mass and central galaxy luminosity are anticorrelated at fixed halo mass. In the case of MOD1, the bright LOWZ cut removes the brightest centrals which are in the most massive haloes causing $N_{\rm cen}(M_{\rm 200b})$ to decrease in higher mass haloes. Grey crosses show MOD1 when the bright cut is not applied – demonstrating that the down-turn in indeed caused by the bright cut. The red curves in the left- and right-hand panels show clustering results from Reid & Spergel (2009) and Parejko et al. (2013), respectively.

BLRG is the central galaxy. This suggests that clusters with non-central BLRGs are not dominated by odd (e.g. merging) clusters.

Previous work has sometimes modelled the distribution of offsets using a Rayleigh distribution function instead of an NFW profile (Johnston et al. 2007):

$$P(d) = \frac{d}{\sigma^2} \exp\left[-\frac{1}{2}\left(\frac{d}{\sigma}\right)^2\right], \quad (26)$$

where $d = D_{\rm off}/R_\lambda$. As shown in Fig. 7, a Rayleigh distribution function with $\sigma = 0.39$ (our best-fitting value) does not provide a satisfactory description of this distribution, although it provides a better fit than an NFW distribution.

4 DISCUSSION ON THE ORIGIN OF THE $N_{\rm cen}$ DISCREPANCY

The above results show that (i) the fraction of redMaPPer clusters with a central LRG ($N_{\rm cen}(\lambda)$) does not converge to unity for rich clusters, (ii) the brightest LRG in a cluster is not the central galaxy in 20–30 per cent of cases, and (iii) the offset distributions of non-central BLRGs are significantly different than that of all cluster members. Below, we put forth possible explanations for why our measured $N_{\rm cen}$ is lower than that inferred from clustering.

4.1 Possible (but unlikely) explanations

One reason that our values for $N_{\rm cen}$ are lower than those found in previous studies might be that the redMaPPer algorithm does not correctly identify central galaxies. We have conducted a visual inspection of 272 redMaPPer clusters in our redshift range. We created colour images for these clusters using the Stripe 82 co-adds (Annis et al. 2014) which are ∼2 mag deeper than the SDSS single epoch imaging. Five co-authors inspected these clusters to select 'visual' central galaxies. Our visual inspection did not reveal any obvious failure modes in the redMaPPer central galaxy selection and we found good agreement between the 'visual' central galaxies and the redMaPPer galaxy with the highest value of $P_{\rm cen}$ (95 per cent of the time). From these tests alone we cannot rule out the possibility that the differences that we find for $N_{\rm cen}$ are due to an incorrect central galaxy assignment by redMaPPer. However, our visual inspections did not reveal any obvious issues. In Paper II we perform tests of the redMaPPer centring probabilities using weak gravitational lensing and cross-correlations. Early results from this work suggest that the redMaPPer centring scheme outperforms other centring choices, such as the bright cluster member.

Based on the above tests, we think that miscentring in the redMaPPer cluster catalogue is unlikely to explain the $N_{\rm cen}$ discrepancy. Another possibility is that part of the difference may be caused by uncertainties in the Rykoff et al. (2012) mass–richness relation. Indeed, the Rykoff et al. (2012) mass–richness relation was derived for an older version of the redMaPPer cluster catalogue. To determine how large of an impact this might have, we use an updated calibration from Reddick et al. (in preparation), which is based on the same redMaPPer catalogue as the one used here.[10] We rederive our results using the updated mass–richness relation but as shown in Fig. 8, this only slightly alters our results. Finally, we also vary $\sigma_{M|\lambda}$ between 0.22 and 0.28 but this does not impact our conclusions. Based on these tests, we conclude that uncertainties in the Rykoff et al. (2012) mass–richness relation are unlikely to explain the discrepancy.

Another possibility is that there is a systematic difference between our photometric LRG selection and the actual spectroscopic samples. However, we obtain similar values for $N_{\rm cen}(\lambda)$ if we select LRGs based on DR7 photometry, or based on the original LRG targeting flag (TARGET_GALAXY_RED, see Appendix A). As discussed

[10] Because Reddick et al. (in preparation) assume a different cosmology than we do, we recalibrate their mass–richness relation for this test. This recalibration yields the same cluster abundances as a function of λ as Reddick et al. (in preparation).

in the Appendix A, differences between our photometric LRG selection and TARGET_GALAXY_RED are consistent with scatter in the photometry between reductions. Hence, differences between the LRG samples from Reid & Spergel (2009) and Parejko et al. (2013) and our photometric LRG selection are unlikely to be the source of the $N_{\rm cen}$ discrepancy.

Another possibility may be related to issues in our conversion from $N_{\rm cen}(\lambda)$ to $N_{\rm cen}(M_{\rm 200b})$. For example, for consistency with Reid & Spergel (2009), we fixed the parameter $\sigma_{\log M}$ to 0.7. However, we have also tested fits with $\sigma_{\log M} = 0.5$ and 0.9. The shape of $N_{\rm cen}(M_{\rm 200b})$ is modified as expected but the overall discrepancy persists. The conversion of $N_{\rm cen}(\lambda)$ to $N_{\rm cen}(M_{\rm 200b})$ also depends on the assumption that $P(M_{\rm 200b}|\lambda)$ follows a log-normal distribution. While this is a very common assumption, it is by no means a well-tested one. It would be interested to test how this assumption would affect our results, but we defer this aspect to future work. Finally, this conversion may also fail if redMaPPer clusters do not represent a perfect recovery of dark matter haloes. If the cluster catalogue contains purity and/or completeness issues, then it will not be safe to assume that one can derive $N_{\rm cen}(M_{\rm 200b})$ from $N_{\rm cen}(\lambda)$. Completeness, however, does not appear to be an issue for the redMaPPer cluster catalogue, beyond the expected scatter in the richness–mass relation, which we have already accounted for in the density matching procedure. Purity, however, is more of a concern. Preliminary X-ray follow-up of a complete sample of redMaPPer clusters suggests that the fraction of redMaPPer clusters that are projections is no larger than 7 per cent. A 7 per cent change in density corresponds to a $\sim$2 per cent change in mass which corresponds to a $\sim$2 per cent change in the scaling relation (Weinberg et al. 2013) and should not dramatically alter our conclusions.

4.2 Implication of our results in terms of central and satellite number densities

In order to compare our results to previous work based on clustering, we compute the number density of central and satellite galaxies implied by our measurements of $N_{\rm cen}(\lambda)$. To compute the central number density, we integrate the product of the best-fitting $N_{\rm cen}(M_{\rm 200b})$ and $\frac{{\rm d}n}{{\rm d}m}(M_{\rm 200b})$ over the full halo mass range. For this calculation, we are forced to extrapolate our model for $N_{\rm cen}(M_{\rm 200b})$ to lower halo masses that are not sampled by the redMaPPer galaxy clusters used here. There is a potentially large systematic uncertainty associated with this extrapolation. On the other hand, the *erf* model in equation (22) is the standard for HOD models. Therefore, any discrepancies between our work and clustering studies that can be traced back to the extrapolation of $N_{\rm cen}(M_{\rm 200b})$ would correspond to a failure in the now standard HOD model. Thus, we simply caution that our conclusions are dependent on the validity of the *erf* extrapolation. Also note that the goal of this exercise is simply to gain a sense of the differences between our results and previous work based on clustering.

Our HOD implies a number density of central galaxies of $1.9 \times 10^{-5}\,{\rm Mpc}^{-3}$ for LRGs and a number density of $4.2 \times 10^{-5}\,{\rm Mpc}^{-3}$ for LOWZ galaxies (see Table 4). Assuming a total number density of $n_{\rm TOT} = 3.4 \times 10^{-5}\,{\rm Mpc}^{-3}$ for LRGs and $n_{\rm TOT} = 1.0 \times 10^{-4}\,{\rm Mpc}^{-3}$ for LOWZ galaxies, we can infer the number density of satellite galaxies ($n_{\rm SAT} = n_{\rm TOT} - n_{\rm CEN}$) and the implied satellite fraction (see Table 4). For LRGs we find that our model implies a satellite number density of $1.5 \times 10^{-5}\,{\rm Mpc}^{-3}$ which corresponds to an LRG satellite fraction of 44 per cent. Likewise, for LOWZ, we find that our model implies a satellite number density of $5.8 \times 10^{-5}\,{\rm Mpc}^{-3}$ which corresponds to a satellite fraction of 58 per cent. These satellite fractions are much higher those of Reid & Spergel (2009) and Parejko et al. (2013), which are 6.4 and 12 per cent, respectively.

The fact that our HOD fits to $N_{\rm cen}(M_{\rm 200b})$ imply much larger satellite fractions than previous works is not surprising because our $N_{\rm cen}(M_{\rm 200b})$ is lower than those of Reid & Spergel (2009) and Parejko et al. (2013). Hence, the satellite fraction must increase in order to preserve the total LRG number density. The satellite fractions derived in this section depend on multiple assumptions and on extrapolating below our halo mass limit. Nonetheless, the satellite fractions inferred from our fits are uncomfortably high – leading us to explore effects that might invalidate our measurements of $N_{\rm cen}(M_{\rm 200b})$. Since our measurements of $N_{\rm cen}(\lambda)$ are reliable (see Section 4.1), we focus on effects that might influence the conversion from $N_{\rm cen}(\lambda)$ to $N_{\rm cen}(M_{\rm 200b})$.

4.3 How would our results be affected by a strong correlation between richness and central luminosity?

Our results rely on converting λ to $M_{\rm 200b}$ via equation (19), which assumes that λ only depends on $M_{\rm 200b}$. Here, we consider the possibility that λ also correlates with $M_I^{\rm CG}$, the absolute magnitude of the central galaxy.

In this case, the conversion in equation (19) will depend on $P(\lambda|M_{\rm 200b}, M_I^{\rm CG})$ instead of just $P(\lambda|M_{\rm 200b})$. To determine how this correlation might impact our results, we evaluate $N_{\rm cen}(M_{\rm 200b})$ for two mock samples in which halo mass and central galaxy luminosity are maximally correlated and anticorrelated, respectively, at fixed richness. We design these samples in the following way.

(i) We build a mock catalogue that contains haloes drawn from the Tinker et al. (2008) mass function. Each halo is assigned a richness based on equation (20).

(ii) We assign an *i*-band central galaxy absolute magnitude to mock haloes. Mock $M_I^{\rm CG}$ values are randomly drawn from the real redMaPPer catalogue after matching mock clusters and real clusters by richness. This procedure ensures that our mock catalogue has the same relationship between λ and $M_I^{\rm CG}$ as the redMaPPer catalogue.

(iii) We then bin the clusters by λ. Each narrow richness bin contains a range of halo masses and central galaxy magnitudes. In the initial catalogue, there is no correlation between $M_I^{\rm CG}$ and $M_{\rm 200b}$. Within each bin, we will *reassign* the $M_I^{\rm CG}$ values in order to introduce a correlation between halo mass and central galaxy magnitude.

(iv) In our first model (MOD1), we reassign all central galaxies such that heavier haloes contain brighter centrals within each richness bin (i.e. $M_{\rm 200b}$ and $M_I^{\rm CG}$ are maximally correlated at fixed λ). In this model, clusters with lower values of λ have brighter central galaxies at fixed halo mass (i.e. λ and $M_I^{\rm CG}$ are *anticorrelated* at fixed halo mass).

(v) In our second model (MOD2), we reassign all centrals galaxies such that heavier haloes contain fainter centrals at fixed richness (i.e. $M_{\rm 200b}$ and $M_I^{\rm CG}$ are maximally anticorrelated at fixed λ). In this model, clusters with lower values of λ have fainter central galaxies at fixed halo mass (i.e. λ and $M_I^{\rm CG}$ are *correlated* at fixed halo mass).

We compute $N_{\rm cen}(M_{\rm 200b})$ for MOD1 and MOD2 and the results are shown in Fig. 8. Interestingly, we find that correlations between halo mass, richness, and central galaxy luminosity may have a *large* impact on our inferences about $N_{\rm cen}(M_{\rm 200b})$. If the magnitude of the central galaxy is maximally correlated with halo mass at fixed richness, then our results would agree with those of Reid & Spergel (2009). For LOWZ galaxies, however, there is a conflicting

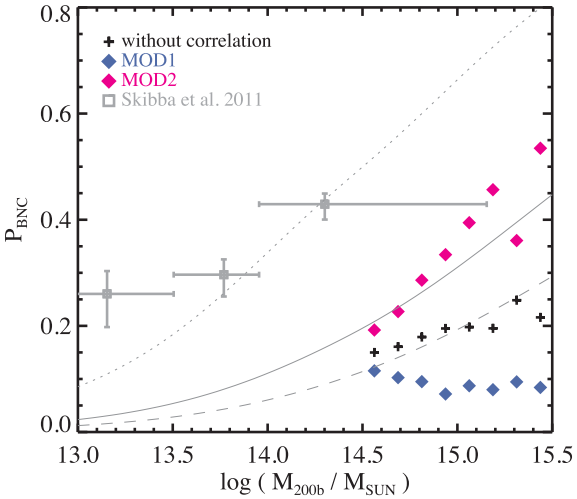

Figure 9. Impact of MOD1 and MOD2 on our inference of $P_{\rm BNC}$. Black plus signs, blue and magenta diamonds represent $P_{\rm BNC}$ values when there is no correlation between central luminosity and cluster richness, and cases of MOD1 and MOD2, respectively. Correlations between central luminosity and cluster richness clearly have a large impact on $P_{\rm BNC}$. The MOD1 model brings our results into closer agreement with Reid & Spergel (2009) but leads to a larger tension with Skibba et al. (2011).

effect due to the bright cut given by equation (15). This cut removes bright galaxies, which, in MOD1, are preferentially located in the most massive haloes. Therefore, $N_{\rm cen}(M_{\rm 200b})$ *decreases* at high halo masses for MOD1. By removing the bright cut, we obtain similar results for the LOWZ and classical LRG samples. However, a fair comparison to Parejko et al. (2013) requires the bright cut for LOWZ selection.

A strong anticorrelation between central luminosity and cluster richness (MOD1) at fixed halo mass would bring our results into good agreement with Reid & Spergel (2009) and $N_{\rm cen}(M_{\rm 200b})$ would converge to unity at large halo masses. It is possible that merging might lead to such an anticorrelation. When a satellite merges with the central galaxy, the richness of the cluster decreases while the magnitude of the central galaxy increases. In this scenario, halo mass estimators based on combinations of $M_I^{\rm CG}$ and λ would result in a smaller scatter than halo mass estimators based on just λ. In fact, Reyes et al. (2008) present evidence this may be the case using the MaxBCG cluster catalogue.

Fig. 8 demonstrates that correlations between central luminosity and cluster richness would clearly impact our inference about $N_{\rm cen}(M_{\rm 200b})$. Fig. 9 also demonstrates that such correlations would also impact our inference of $P_{\rm BNC}$. To match the Reid & Spergel (2009) result, we must assume that central galaxy luminosity and cluster richness are strongly anticorrelated. While such a strong anticorrelation seems unlikely, preliminary results from Reddick et al. (in preparation) based on an analysis of the conditional luminosity function (CLF) of redMaPPer cluster members also suggest a strong anticorrelation between richness and central galaxy luminosity.

In conclusion, a strong anticorrelation between central luminosity and cluster richness at fixed halo mass is required in order to reconcile our results with those based on clustering studies. However, further investigation is needed to confirm or repudiate this hypothesis. An interesting direction for future work will be follow-up on our study by performing a *joint* CLF analysis of LRG clustering, galaxy–galaxy lensing, and direct counts in clusters (Tinker et al. 2012).

4.4 How robust is $N_{\rm cen}$ inferred from clustering and CIC studies?

Finally, we note that the values of $N_{\rm cen}$ from studies similar to Reid & Spergel (2009) that use observables such as counts-in-cylinders or clustering could be dominated by theoretical prejudices. For example, at the low-mass end, HOD models often make the standard assumption that a halo cannot host a satellite galaxy if it does not also host a central galaxy from the same sample. Under this assumption, most LRGs in low-mass haloes (which contain on average only one LRG or less) will be centrals. But given that observations of counts-in-cylinders probe $N_{\rm tot}$ they should not be able distinguish between this standard scenario and a scenario in which a fraction of LRGs in low-mass haloes are in fact satellites.

The clustering signal may also be relatively insensitive to such effects. In these small haloes there are no central–satellite or satellite–satellite pairs of galaxies. Therefore, the difference in the clustering between the two scenarios will arise only due to galaxy pairs in two different haloes (the two-halo term), which also may not be heavily affected. In particular, if non-central LRGs in low-mass haloes follow a radial distribution peaked towards the centre as shown in Fig. 7, the differences in the clustering signal may be small.

Similar arguments hold at the high-mass end. HOD models often assume that $N_{\rm cen}$ approaches unity at large halo masses. At these mass scales, the one-halo term in the clustering signal is dominated by the satellite–satellite term (which is not sensitive to $N_{\rm cen}$), except possibly at the smallest scales where the observational uncertainties are significantly larger (Masjedi et al. 2006). As argued before, counts-in-cylinders will not be able to make a distinction between centrals and satellites either.

The effect of the above theoretical prejudices on the $N_{\rm cen}$ constraints obtained from studies relying on counts-in-cylinders or clustering can be studied in detail using mock galaxy catalogues. Such an investigation, however, is beyond the scope of the current paper, and is left for future work.

5 SUMMARY AND CONCLUSIONS

In this paper, we investigate the connection between central galaxies in clusters and two classes of red luminous spectroscopic galaxies: 'classical LRGs', which were targeted as part of the SDSS-I and SDSS-II programs (Eisenstein et al. 2001), and LOWZ galaxies from the SDSS-III BOSS program (Dawson et al. 2013). The aim of this paper is to address two different questions: (i) what fraction of cluster central galaxies are classified as either an LRG or a LOWZ galaxy, and (ii) when a central cluster galaxy is either a LRG or a LOWZ galaxy, how often is the central galaxy also the brightest LRG in the cluster.

To tackle these two questions, we use the state-of-the art redMaPPer cluster catalogue in the redshift range $0.16 < z < 0.33$ and in the richness range $\lambda > 20$, corresponding to a halo masses above $2.44 \times 10^{14}\,{\rm M}_{\odot}$. To avoid complications due to fibre collisions, we construct a set of photometric LRG/LOWZ cluster members. Extensive tests show that these photometric samples are in excellent agreement with the original LRG and LOWZ target catalogues (>95 per cent, see the appendix).

A key feature of the redMaPPer cluster catalogue is that it defines cluster members and central galaxies probabilistically. Using the centring probabilities given by redMaPPer, we derive the central occupation of LRGs and LOWZs as a function of richness, $N_{\rm cen}(\lambda)$, and halo mass, $N_{\rm cen}(M_{\rm 200b})$. We find the striking result that the central occupation function for both classical LRGs and

LOWZ galaxies does not converge to unity, even for large clusters. Instead, $N_{\rm cen}(\lambda)$ converges to $\sim$0.95. This can be explained by the large scatter in central galaxy luminosity at fixed richness and the LRG/LOWZ selection cuts, which both impose absolute magnitude limits that exclude central galaxies in the redMaPPer catalogue.

When we naively convert $N_{\rm cen}(\lambda)$ into $N_{\rm cen}(M_{\rm 200b})$, assuming that the halo mass only depends on cluster richness, the central occupation still only converges to 0.95 for massive haloes. This is in conflict with the assumptions behind most HOD-type studies of the two-point correlation function.

While inaccuracies in the redMaPPer centroids could cause this discrepancy, we will show in Paper II that the redMaPPer centring probabilities are reliable. Instead, we show that if the magnitude of the central galaxy is maximally correlated with halo mass at fixed richness (i.e. λ and $M_I^{\rm CG}$ are *anticorrelated* at fixed halo mass), then our results for 'classical' LRGs would agree with those of Reid & Spergel (2009). This maximal anticorrelation does not alleviate the tension between our results for LOWZ galaxies and those of Parejko et al. (2013). This is because the LOWZ selection includes a bright cut, and, by correlating galaxy brightness and halo mass, we systematically lower the fraction of central LOWZ galaxies in massive haloes, thus decreasing $N_{\rm cen}(M_{\rm 200b})$ for massive clusters.

Our results may indicate a strong correlation between central galaxy luminosity and halo mass at fixed cluster richness. This is equivalent to a strong *anticorrelation* between central galaxy brightness and richness at fixed halo mass. It is possible that merging might lead to this anticorrelation: mergers between satellite galaxies and the central galaxy will increase the central galaxy luminosity and decrease the cluster richness. In fact, examples of the extreme cases of such a correlation have been well studied and are known as 'fossil groups' (e.g. Jones et al. 2003; D'Onghia et al. 2005; Zentner et al. 2005). However, further investigation will be necessary in order to confirm if this correlation may be strong enough to fully explain our results. Another possibility is that the HOD models from counts-in-cylinders or clustering may be subject to theoretical prejudices in this high halo mass regime. It is possible that the differences that we observe for the central occupation function may be caused by a combination of both effects. An interesting direction for future work will be to try to disentangle these effects by performing a *joint* CLF analysis of LRG clustering, galaxy–galaxy lensing, and direct counts in clusters as in Tinker et al. (2012).

We also investigate how often the brightest cluster member is not the central galaxy, $P_{\rm BNC}$. Using both the cluster member probabilities and the central galaxy probabilities from redMaPPer, we find that in 20–30 per cent of clusters the brightest galaxy is not the central galaxy. Our estimate is in good agreement with a CLF analysis by Reddick et al. (in preparation), but our measurement of $P_{\rm BNC}$ is nearly a factor of 2 lower than that of Skibba et al. (2011). The large discrepancy with Skibba et al. (2011) may be in part due to improvements in the SDSS sky subtraction between DR4 (used by Skibba et al. 2011) and DR8 (used here). Reddick et al. (in preparation) demonstrate that improved sky subtraction around luminous, extended galaxies tends to increase the difference in luminosity between central and satellite galaxies, thus substantially decreasing $P_{\rm BNC}$. However, further testing is required to determine if the differences in photometry apply to galaxies in the redshift range studied here. We have also quantified the radial distribution of bright non-central LRGs and found that they follow a substantially different distribution (truncated at the outskirts) compared to the distribution for all cluster members.

Because we find a significant fraction of clusters in which the BLRG is not the central galaxy, using the brightest galaxy as a tracer for the cluster centre will lead to errors due to 'miscentring', particularly in RSD studies based on LRG 'halo catalogues' (e.g. Reid et al. 2010; Hikage et al. 2013). The analysis in Hikage et al. (2013) suggests a miscentring fraction for BLRGs of 30–40 per cent, in rough agreement with the 20–30 per cent miscentring we find above. Hikage et al. (2013) demonstrate that miscentring of this magnitude may significantly affect cosmological parameter estimation in future surveys, such as Extended Baryon Oscillation Spectroscopic Survey (eBOSS), Prime Focus Spectrograph (PFS), and Dark Energy Spectroscopic Instrument (DESI). Future work will investigate how well the BLRG satellite population can be characterized using a joint analysis of BLRG clustering and information from cluster catalogues, such as redMaPPer. By characterizing satellite BLRGs, the effects of miscentring may be mitigated.

The results presented here rely on the assumption that the probability values from redMaPPer, particularly those for the cluster centre, are accurate. A comparison of X-ray to optical centres in galaxy clusters with available data suggests that the redMaPPer centring probabilities are indeed accurate (Rozo & Rykoff 2014). However, the sample sizes for these comparisons are still small, and rely heavily on X-ray selected subsamples of clusters. More detailed investigation into the redMaPPer centring probabilities is warranted. Following the methods of George et al. (2012) and Hikage et al. (2013), in Paper II, we will perform tests of the redMaPPer centring probabilities by using a combination of weak gravitational lensing and the projected correlation between the LRG-inferred haloes and a fainter photometric sample of galaxies. Preliminary results from Paper II indicate that the redMaPPer centroids are better tracers of halo centres than the brightest cluster members. This lends credence to both the redMaPPer centring probabilities, and the results presented in this work.

In conclusion, LRGs are considered among the best understood samples of galaxies and are expected to occupy haloes in a relatively simple way. However, in this paper we have shown that even these relatively simple galaxies still harbour surprises and that the connection between LRGs and dark matter haloes may not be straightforward.

ACKNOWLEDGEMENTS

We thank Tamas Budavari for helping us with querying the SDSS data base. Jeremy Tinker kindly provided us with the LOWZ target catalogue, and Naoshi Sugiyama supported us with helpful discussions. We thank the anonymous referee for useful comments that helped improve this paper. AL, CL, AM, SM, SS, and BV were supported by World Premier International Research Center Initiative (WPI Initiative), MEXT, Japan. RM acknowledges the support of the Department of Energy Early Career Award program. BV was supported by the Kakenhi Grant-in-Aid for Young Scientists (B)(26870140) from the Japan Society for the Promotion of Science (JSPS). AM was supported by a research fellowship from the Japan Society for the Promotion of Science (JSPS).

REFERENCES

Abazajian K. N. et al., 2009, ApJS, 182, 543
Aihara H. et al., 2011, ApJS, 193, 29
Annis J. et al., 2014, ApJ, 794, 120
Berlind A. A., Weinberg D. H., 2002, ApJ, 575, 587
Bernardi M., Meert A., Sheth R. K., Vikram V., Huertas-Company M., Mei S., Shankar F., 2013, MNRAS, 436, 697
Blanton M. R., Roweis S., 2007, AJ, 133, 734

Budzynski J. M., Koposov S. E., McCarthy I. G., McGee S. L., Belokurov V., 2012, MNRAS, 423, 104
Cabré A., Gaztañaga E., 2009, MNRAS, 393, 1183
Cacciato M., van den Bosch F. C., More S., Li R., Mo H. J., Yang X., 2009, MNRAS, 394, 929
Cacciato M., van den Bosch F. C., More S., Mo H., Yang X., 2013, MNRAS, 430, 767
Coziol R., Andernach H., Caretta C. A., Alamo-Martínez K. A., Tago E., 2009, AJ, 137, 4795
Dawson K. S. et al., 2013, AJ, 145, 10
D'Onghia E., Sommer-Larsen J., Romeo A. D., Burkert A., Pedersen K., Portinari L., Rasmussen J., 2005, ApJ, 630, L109
Einasto M. et al., 2011, ApJ, 736, 51
Einasto M. et al., 2012, A&A, 540, A123
Eisenstein D. J. et al., 2001, AJ, 122, 2267
Eisenstein D. J. et al., 2005, ApJ, 633, 560
George M. R. et al., 2012, ApJ, 757, 2
Hansen S. M., McKay T. A., Wechsler R. H., Annis J., Sheldon E. S., Kimball A., 2005, ApJ, 633, 122
Hikage C., Yamamoto K., 2013, J. Cosmol. Astropart. Phys., 8, 19
Hikage C., Mandelbaum R., Takada M., Spergel D. N., 2013, MNRAS, 435, 2345
Ho S., Lin Y.-T., Spergel D., Hirata C. M., 2009, ApJ, 697, 1358
Johnston D. E. et al., 2007, preprint (arXiv:0709.1159)
Jones L. R., Ponman T. J., Horton A., Babul A., Ebeling H., Burke D. J., 2003, MNRAS, 343, 627
Kazin E. A. et al., 2010, ApJ, 710, 1444
Koester B. P. et al., 2007, ApJ, 660, 239
Lauer T. R., Postman M., Strauss M. A., Graves G. J., Chisari N. E., 2014, ApJ, 797, 82
Leauthaud A. et al., 2010, ApJ, 709, 97
Mandelbaum R., Seljak U., Cool R. J., Blanton M., Hirata C. M., Brinkmann J., 2006, MNRAS, 372, 758
Masjedi M. et al., 2006, ApJ, 644, 54
Miyatake H. et al., 2013, preprint (arXiv:1311.1480)
More S., Kravtsov A. V., Dalal N., Gottlöber S., 2011, ApJS, 195, 4
More S., van den Bosch F. C., Cacciato M., More A., Mo H., Yang X., 2013, MNRAS, 430, 747
More S., Miyatake H., Mandelbaum R., Takada M., Spergel D., Brownstein J., Schneider D. P., 2014, preprint (arXiv:1407.1856)
Padmanabhan N. et al., 2008, ApJ, 674, 1217
Padmanabhan N., White M., Norberg P., Porciani C., 2009, MNRAS, 397, 1862
Parejko J. K. et al., 2013, MNRAS, 429, 98
Peacock J. A., Smith R. E., 2000, MNRAS, 318, 1144
Reid B. A., Spergel D. N., 2009, ApJ, 698, 143
Reid B. A., Spergel D. N., Bode P., 2009, ApJ, 702, 249
Reid B. A. et al., 2010, MNRAS, 404, 60
Reyes R., Mandelbaum R., Hirata C., Bahcall N., Seljak U., 2008, MNRAS, 390, 1157
Rozo E., Rykoff E. S., 2014, ApJ, 783, 80
Rozo E., Rykoff E. S., Bartlett J. G., Melin J. B., 2014a, preprint (arXiv:1401.7716)
Rozo E., Rykoff E. S., Becker M., Reddick R. M., Wechsler R. H., 2014b, preprint (arXiv:1410.1193)
Rykoff E. S. et al., 2012, ApJ, 746, 178
Rykoff E. S. et al., 2014, ApJ, 785, 104
Samushia L., Percival W. J., Raccanelli A., 2012, MNRAS, 420, 2102
Sanderson A. J. R., Edge A. C., Smith G. P., 2009, MNRAS, 398, 1698
Schlegel D. J., Finkbeiner D. P., Davis M., 1998, ApJ, 500, 525
Scoccimarro R., Sheth R. K., Hui L., Jain B., 2001, ApJ, 546, 20
Sehgal N. et al., 2013, ApJ, 767, 38
Seljak U., 2000, MNRAS, 318, 203
Skibba R. A., van den Bosch F. C., Yang X., More S., Mo H., Fontanot F., 2011, MNRAS, 410, 417
Strauss M. A. et al., 2002, AJ, 124, 1810
Tinker J., Kravtsov A. V., Klypin A., Abazajian K., Warren M., Yepes G., Gottlöber S., Holz D. E., 2008, ApJ, 688, 709
Tinker J. L. et al., 2012, ApJ, 745, 16
van den Bosch F. C., Norberg P., Mo H. J., Yang X., 2004, MNRAS, 352, 1302
van den Bosch F. C., Weinmann S. M., Yang X., Mo H. J., Li C., Jing Y. P., 2005, MNRAS, 361, 1203
van den Bosch F. C., More S., Cacciato M., Mo H., Yang X., 2013, MNRAS, 430, 725
Weinberg D. H., Mortonson M. J., Eisenstein D. J., Hirata C., Riess A. G., Rozo E., 2013, Phys. Rep., 530, 87
Weinmann S. M., van den Bosch F. C., Yang X., Mo H. J., 2006, MNRAS, 366, 2
Wu H.-Y., Hahn O., Evrard A. E., Wechsler R. H., Dolag K., 2013, MNRAS, 436, 460
Yang X., Mo H. J., van den Bosch F. C., Pasquali A., Li C., Barden M., 2007, ApJ, 671, 153
York D. G. et al., 2000, AJ, 120, 1579
Zehavi I. et al., 2005, ApJ, 621, 22
Zentner A. R., Berlind A. A., Bullock J. S., Kravtsov A. V., Wechsler R. H., 2005, ApJ, 624, 505
Zheng Z. et al., 2005, ApJ, 633, 791

APPENDIX A: OUR PHOTOMETRIC SAMPLE AND SDSS TARGET SELECTION

Our LRG sample selection is described in Section 2.2. Here, we compare this sample to the actual LRG sample targeted for spectroscopy in SDSS (Eisenstein et al. 2001). Although the cuts described above are the same as those for the targeted sample, the SDSS photometry changed slightly between DR7 and DR8. As we show below, this slightly alters our LRG sample when compared to the targeted sample. To do this comparison, we introduce the following new samples:

(i) DR7PhotLRG: photometrically selected LRGs with DR7 photometry;
(ii) TargLRG: original set of LRGs that are targeted by SDSS;
(iii) TargLOWZ: original set of LOWZs that are targeted by SDSS.

A1 DR8PhotLRG, DR7PhotLRG, and TargLRG

The SDSS LRGs selected for spectroscopy are flagged `TARGET_GALAXY_RED`, and we queried DR7 to get all such galaxies. We call these SDSS LRGs 'TargLRGs'. These galaxies are selected using the cuts described in Section 2.3, but using earlier reductions of the SDSS data.

We note here that there is an implicit bright cut in TargLRG, due to the bright cut in the SDSS main sample, which is not part of our photometric LRG selection. The bright limit is included because very bright objects may cause contamination of spectra or saturation of the CCDs. Galaxies with apparent magnitudes brighter than 15 in g or r band or 14.5 in i band, or Petrosian magnitudes brighter than $r_{\rm Petro} < 15$ are excluded from SDSS main sample, and, therefore from TargLRG. However, since every galaxy in our redMaPPer cluster catalogue is fainter than this limit, the bright limit for classical LRGs is not relevant to our work.

We compare TargLRG to our sample of photometrically selected LRGs, DR8PhotLRG. Since the DR8 sky coverage is wider than that of DR7, we do the comparison in a region where DR8 and DR7 overlap, i.e. the North Galactic Cap. However, we find that the TargLRG sample contains holes in this region, due to missing runs. Therefore, we restrict our comparison to smaller region in the North Galactic Cap: $120 < {\rm RA} < 250$ and $20 < {\rm Dec.} < 50$. In this region, there are 3549 DR8PhotLRGs and 3542 TargLRGs; 3191 galaxies

are in both samples, which is 89.9 per cent of the DR8PhotLRG sample and 90.1 per cent of TargLRG sample.

We perform the same comparison, replacing DR8PhotLRGs with DR7PhotLRGs. These samples are selected identically, but the latter uses DR7 photometry. Since the LRG target catalogue was made before DR8, and there are small changes in the photometry between DR8 and earlier data releases, it is worthwhile to compare TargLRGs with DR7PhotLRGs. Here we again take the region limited by $120 < \mathrm{RA} < 250$ and $20 < \mathrm{Dec.} < 50$ in the North Galactic Cap so as not to be affected by missing runs in TargLRG. In this region, there are 3532 DR7PhotLRGs and 3542 TargLRGs. The samples overlap for 3323 galaxies, which is 97.9 per cent of DR7PhotLRG and 97.7 per cent of TargLRG.

In conclusion, when we use DR7 photometry, we find a 6 per cent difference between the original LRG target catalogue and our photometric selection. When we use DR8 photometry, the difference increases to 12 per cent. This demonstrates, that while similar, our classical LRG sample is not identical to the SDSS spectroscopic LRG sample and care must be taken when comparing the two. The source of these differences is likely scatter in the photometry between reductions. Directly comparing DR7 and DR8 photometry for the same galaxies, we find the rms scatter in the magnitudes and colours is $\sim$0.07 mag, with no systematic offsets. Photometric scatter will affect faint LRGs more than bright LRGs. Reassuringly, when comparing TargLRG, DR7PhotLRG, and DR8PhotLRG, galaxies in one sample but not the others are on average half a magnitude fainter than typical LRGs. Photometric scatter mainly affects the LRG sample near the colour–magnitude cuts for LRG selection, but the overall number of LRGs selected in each sample is nearly unchanged. Therefore, while the samples of LRGs cannot be directly compared, they are equivalent for our analysis.

A2 BOSS LOWZ target selection

As with classical LRGs, we compare our original PhotLOWZs to the LOWZ target catalogue. For the LOWZ target catalogue, we use 'bosstarget-lrg-main007-collate.fits'.[11] This catalogue contains LOWZ galaxies, as well as CMASS-selected galaxies at higher redshifts ($0.4 < z < 0.7$). We select LOWZ galaxies with the flag

(boss_target1 AND 2^0) NE 0.

We call the LOWZs in the target catalogue 'TargLOWZs'. Before comparing TargLOWZs and PhotLOWZs, we need to remove regions with problems in the target catalogue. Because of a bug in the star–galaxy separation used to create the target catalogue, there are some regions we need to exclude. To remove undesired regions, we remove objects from TargLOWZ with

TILE < 10324.

Then we simply take the regions that are not affected by this bug. They are

(i) $0 < \mathrm{RA} < 50$, $2 < \mathrm{Dec.} < 40$;
(ii) $140 < \mathrm{RA} < 270$, $45 < \mathrm{Dec.} < 70$;
(iii) $100 < \mathrm{RA} < 220$, $6 < \mathrm{Dec.} < 28$;
(iv) $310 < \mathrm{RA} < 360$, $-15 < \mathrm{Dec.} < 40$.

There are 12 778 PhotLOWZs in these regions, 12 294 of which (96.2 per cent) are also selected as TargLOWZ. As with classical LRGs, the photometric LOWZ selection closely mimics the actual spectroscopic LOWZ sample. The small differences can be explained by small changes in the photometry used for target selection over the course of the BOSS survey.

[11] http://www.sdss3.org/dr10/algorithms/boss_target_selection.php

APPENDIX B: SDSS QUERIES

B1 How to get photometric properties from DR8

To obtain data from SDSS, we used the SDSS CASJOBS tool.[12] First, we match objects from the redMaPPer catalogue to SDSS data in RA and Dec. using a 1.5 arcsec match radius. The results of this match are stored in MATCHTABLE. We select the properties of the matched redMaPPer galaxies from SDSS DR8 using the SQL query:

```
SELECT
matchtable.search_id, matchtable.ra,
matchtable.dec, p.modelMag_r, p.modelmag_i,
p.modelmag_g, p.modelmag_z, p.modelmag_u,
p.modelmagerr_u, p.modelmagerr_g, p.modelmagerr_r,
p.modelmagerr_i, p.modelmagerr_z, p.cmodelMag_r,
p.cmodelmag_i, p.cmodelmag_g, p.cmodelmag_z,
p.cmodelmag_u, p.cmodelmagerr_u, p.cmodelmagerr_g,
p.cmodelmagerr_r, p.cmodelmagerr_i,
p.cmodelmagerr_z, p.extinction_r, p.extinction_i,
p.extinction_g, p.extinction_z, p.extinction_u,
p.petromag_r, p.psfmag_r, p.petror50_r,
p.devrad_i, p.flags, p.objid
INTO mydb.outputtable
FROM mydb.matchtable
JOIN PhotoPrimary as p on matchtable.matched_id=
p.objid
ORDER BY matchtable.search_id
```

B2 How to get actual LRG target from SDSS

To get the SDSS DR7 LRG target catalogue (TargLRGs), we queried the SDSS DR7 database for all galaxies flagged as TARGET_GALAXY_RED:

```
SELECT
run, camCol, rerun, field, objID, ra, dec,
modelmag_u, modelmag_g, modelmag_r, modelmag_i,
modelmag_z, modelmagerr_u, modelmagerr_g,
modelmagerr_r, modelmagerr_i, modelmagerr_z,
extinction_u, extinction_g, extinction_r,
extinction_i, extinction_z, petromag_r, psfmag_r,
petror50_r, devrad_i
into mydb.DR7_LRG_all
from TargPhotoPrimary
WHERE (primtarget &
dbo.fPrimTarget('TARGET_GALAXY_RED')) != 0
```

[12] http://skyserver.sdss3.org/CasJobs/

This paper has been typeset from a TEX/LATEX file prepared by the author.